

## Global calibration of novel 3-hydroxy fatty acid based temperature and pH proxies

Wang, Canfa; Bendle, James A.; Yang, Huan; Yang, Yi; Hardman, Alice; Yamoah, Afrifa; Thorpe, Amy; Mandel, Ilya; Greene, Sarah E.; Huang, Junhua; Xie, Shucheng

DOI:  
[10.1016/j.gca.2021.03.010](https://doi.org/10.1016/j.gca.2021.03.010)

License:  
Creative Commons: Attribution-NonCommercial-NoDerivs (CC BY-NC-ND)

*Document Version*  
Peer reviewed version

*Citation for published version (Harvard):*  
Wang, C, Bendle, JA, Yang, H, Yang, Y, Hardman, A, Yamoah, A, Thorpe, A, Mandel, I, Greene, SE, Huang, J & Xie, S 2021, 'Global calibration of novel 3-hydroxy fatty acid based temperature and pH proxies', *Geochimica et Cosmochimica Acta*, vol. 302, pp. 101-119. <https://doi.org/10.1016/j.gca.2021.03.010>

[Link to publication on Research at Birmingham portal](#)

### General rights

Unless a licence is specified above, all rights (including copyright and moral rights) in this document are retained by the authors and/or the copyright holders. The express permission of the copyright holder must be obtained for any use of this material other than for purposes permitted by law.

- Users may freely distribute the URL that is used to identify this publication.
- Users may download and/or print one copy of the publication from the University of Birmingham research portal for the purpose of private study or non-commercial research.
- User may use extracts from the document in line with the concept of 'fair dealing' under the Copyright, Designs and Patents Act 1988 (?)
- Users may not further distribute the material nor use it for the purposes of commercial gain.

Where a licence is displayed above, please note the terms and conditions of the licence govern your use of this document.

When citing, please reference the published version.

### Take down policy

While the University of Birmingham exercises care and attention in making items available there are rare occasions when an item has been uploaded in error or has been deemed to be commercially or otherwise sensitive.

If you believe that this is the case for this document, please contact [UBIRA@lists.bham.ac.uk](mailto:UBIRA@lists.bham.ac.uk) providing details and we will remove access to the work immediately and investigate.

1           **Global calibration of novel 3-hydroxy fatty acid based temperature and pH**  
2   **proxies**

3

4   Canfa Wang<sup>a</sup>, James A. Bendle<sup>b</sup>, Huan Yang<sup>c</sup>, Yi Yang<sup>c</sup>, Alice Hardman<sup>b</sup>, Afrifa  
5   Yamoah<sup>b</sup>, Amy Thorpe<sup>b</sup>, Ilya Mandel<sup>d,e,f</sup>, Sarah E. Greene<sup>b</sup>, Junhua Huang<sup>g</sup>, Shucheng  
6   Xie<sup>a</sup>

7   <sup>a</sup> State Key Laboratory of Biogeology and Environmental Geology, Hubei Key  
8   Laboratory of Critical Zone Evolution, China University of Geosciences, Wuhan,  
9   430074, China

10  <sup>b</sup> School of Geography, Earth and Environmental Sciences, University of Birmingham,  
11  Birmingham, B15 2TT, UK

12  <sup>c</sup> School of Geography and Information Engineering, China University of Geosciences,  
13  Wuhan 430074, China

14  <sup>d</sup> School of Physics and Astronomy, Monash University, VIC 3800, Australia

15  <sup>e</sup> OzGrav: The Australian Research Council Centre of Excellence for Gravitational  
16  Wave Discovery, Clayton, VIC 3800, Australia

17  <sup>f</sup> Birmingham Institute for Gravitational Wave Astronomy and School of Physics and  
18  Astronomy, University of Birmingham, Birmingham B15 2TT, UK

19  <sup>g</sup> State Key Laboratory of Geological Processes and Mineral Resources, China  
20  University of Geosciences, Wuhan, 430074, China

21

22

23

24 **Abstract**

25 3-Hydroxy fatty acids (3-OH-FAs), derived from Gram-negative bacterial outer  
26 membranes, have received recent attention for their potential as new terrestrial pH and  
27 temperature proxies for palaeoclimate studies. Initial studies from altitudinal transects  
28 of contemporary soils - correlating bacterial 3-OH-FA compositions to air temperature  
29 and pH - have shown promising results. But the geographical extent of recent  
30 calibrations is limited. In this study, we analyse 3-OH-FA lipid distributions in 186  
31 globally distributed soil samples to study the environmental factors controlling the  
32 relative distribution of the 3-OH-FA isomers. Our sample-set covers a wide range of  
33 temperatures (-0.4 to 27°C) and pH (3.6 to 9.2). For the global compilation we find  
34 that the ratio of *anteiso* to *normal* 3-OH-FAs of the C<sub>15</sub> or C<sub>17</sub> homologues (RAN<sub>15</sub> or  
35 RAN<sub>17</sub>) shows a strong linear relationship with mean annual air temperature (MAAT)  
36 ( $R^2=0.48$ ,  $p < 0.001$  and  $R^2 = 0.41$ ,  $p < 0.001$ , respectively). Additionally, the negative  
37 logarithm of the ratio of the summed *iso* and *anteiso* to the total amount of *normal* 3-  
38 OH-FAs (RIAN) is also strongly anticorrelated with the soil pH ( $R^2 = 0.66$ ,  $p < 0.001$ ).  
39 However, we find that for our 3-OH-FA based proxies there are significant differences  
40 in slope and intercept of the linear corrections at regional scales. Thus local or regional  
41 calibrations are likely preferable (at this stage of 3-OH-FA proxy development) for  
42 application to specific palaeoclimate archives. We also explore the relationship of 3-  
43 OH-FA isomer fractional abundances to environmental parameters using machine  
44 learning tools (a Gaussian Process (GP) emulator). This confirms the first order  
45 relationships to environmental parameters highlighted by the empirical equations and  
46 also derives several alternative GP emulator models for reconstructing MAAT and pH  
47 which give higher  $R^2$  values (0.66 for MAAT; 0.63 for pH) and lower RSME values  
48 (3.5°C for MAAT; 0.76 for pH) compared to simple linear regressions at the global

49 scale. We compare our 3-OH-FA based indices with bacterial branched glycerol dialkyl  
50 glycerol tetraethers (brGDGTs) based indices from the same soil samples. At a global  
51 scale RAN<sub>15</sub> and RAN<sub>17</sub> show negative correlations with the MBT'<sub>5ME</sub>-MAAT (MBT'  
52 <sub>5ME</sub>, methylation index of 5-methyl branched tetraethers) ( $r = -0.59, p < 0.001$  and  $r =$   
53  $-0.42, p < 0.001$ , respectively), whilst RIAN shows strong linear correlations with the  
54 cyclisation ratio of branched tetraethers (CBT) ( $r = 0.77, p < 0.001$ ). Similar to 3-OH-  
55 FA based temperature proxies, GDGT based temperature proxy MBT'<sub>5ME</sub> also showed  
56 different regional calibrations. Our new field-based correlations demonstrate the broad  
57 physiological response of Gram-negative bacterial cell membranes to external  
58 environmental changes on a global scale. We suggest that 3-OH-FA based proxies have  
59 widespread potential for palaeoenvironmental studies to estimate past MAAT and soil  
60 pH, but that regional/ local and context specific calibrations may need to be applied.

61

62 **Keywords:** 3-Hydroxy fatty acid; 3-OH-FA; Soils; Proxies; Temperature; pH;

63 Palaeoclimate; Biomarkers

64

## 65 **1. Introduction**

66 Instrumental records, satellite observations and laboratory studies do not cover the  
67 likely amplitude or patterns of response of Earth's climate and carbon system to the  
68 extreme climate forcing expected this century (IPCC, 2014). Reconstruction of past  
69 climate change, beyond the scope of meteorological records, is critical for providing  
70 natural baselines, improving understanding of the Earth system and predicting future  
71 change. A wide range of environmental information from both terrestrial and marine

72 realms is required from palaeoclimate archives for this endeavour. Microbial lipids are  
73 sensitive to ambient environmental changes. A number of organic geochemical proxies  
74 based on microbial lipids have been developed for palaeoclimate reconstruction  
75 (Eglinton and Eglinton, 2008; Luo et al., 2019; Meyers, 1997; Schouten et al., 2013).  
76 Three lipid biomarker based indices, TEX<sub>86</sub> (Kim et al., 2008; Schouten et al., 2002),  
77 U<sub>37</sub><sup>K</sup> (Brassell et al., 1986; Haug et al., 2005; Prahl and Wakeham, 1987; Sachs et al.,  
78 2001) and LDI (de Bar et al., 2020; Naafs et al., 2012; Rampen et al., 2012) have  
79 become important tools for determination of past sea surface temperature (SST).  
80 However, the above-mentioned proxies are generally applied in marine settings and  
81 biomarker based proxies for terrestrial environments, especially for temperature,  
82 remain relatively scarce. This is unfortunate as the terrestrial environment is where the  
83 climate change impacts will most affect human societies. Bacterial branched glycerol  
84 dialkyl glycerol tetraethers (brGDGTs) are the primary biomarker based proxy for  
85 temperature and pH (Peterse et al., 2012; Weijers et al., 2007) currently applied to  
86 terrestrial archives (Schouten et al., 2013 and references therein). Using improved  
87 chromatographic separation, a new temperature proxy MBT'<sub>5ME</sub> was defined, which is  
88 pH independent and reduces the residual mean error (RMSE) for mean annual air  
89 temperature (MAAT) reconstructions (De Jonge et al., 2013; De Jonge et al., 2014;  
90 Hopmans et al., 2016). However, the utility of GDGT based approaches is still limited  
91 by uncertainties over the biological source (Weber et al., 2015), *in-situ* production and  
92 transport of brGDGTs in lake settings (Blaga et al., 2010). We note that several novel  
93 terrestrial bacterial biomarker based proxies have been recently proposed, namely the  
94 branched fatty alcohol ratio BNA<sub>15</sub> (Huang et al., 2013) and several proxies based on  
95 heterocyst glycolipids (HG<sub>28</sub> and HG<sub>30</sub>) (Bauersachs et al., 2015; Klages et al., 2020).  
96 The BNA<sub>15</sub>, HG<sub>28</sub> and HG<sub>30</sub> proxies show promise but have yet to be globally calibrated

97 and widely applied. Finally, neither GDGTs nor HGs are readily amenable to isotopic  
98 analyses using standard methods, limiting potential insights to the terrestrial carbon and  
99 hydrological cycles. We seek to overcome these limitations by developing a new suite  
100 of terrestrial palaeoclimatic proxies that can reconstruct temperature and pH  
101 independently (and which have the future potential to yield isotopic information using  
102 routine analytical approaches). Thus, further development of novel terrestrial proxies,  
103 independent and complementary to GDGTs, is needed to expand applications and  
104 improve the reliability and accuracy of terrestrial environmental reconstructions.

105 Gram-negative bacterial membrane derived 3-hydroxy fatty acids (3-OH-FAs)  
106 have the potential to be developed as environmental proxies. 3-OH-FAs with carbon  
107 numbers from C<sub>10</sub> to C<sub>18</sub> are primarily derived from lipid A, a constituent of  
108 lipopolysaccharide (LPS), the main component of the outer membrane of Gram-  
109 negative bacteria (Szponar et al., 2003; Szponar et al., 2002; Wollenweber and  
110 Rietschel, 1990). Gram-negative derived 3-OH-FAs are bound to the glucosamine unit  
111 of lipid A either by ester bonds or amide bonds (Kumar et al., 2002; Raetz et al., 2007;  
112 Wollenweber and Rietschel, 1990). Acid digestion is a more appropriate method than  
113 saponification to extract them from soil and stalagmite samples (Wang et al., 2016;  
114 Yang et al., 2016). So far 3-OH-FAs have been found in soils (Huguet et al., 2019;  
115 Wang et al., 2016; Zelles, 1999), speleothems (Blyth et al., 2006; Huang et al., 2008;  
116 Wang et al., 2018; Wang et al., 2012), snow (Tyagi et al., 2016; Tyagi et al., 2015),  
117 aerosols (Lee et al., 2004), marine dissolved organic matter (DOM) (Wakeham et al.,  
118 2003), marine and lake sediments (Kawamura and Ishiwatari, 1984; Volkman et al.,  
119 1980; Wakeham, 1999; Wang et al., 2016; Yang et al., 2020; Zhang et al., 2014), and a  
120 3-OH-FA based proxy for sea surface temperature (RAN<sub>13</sub>) has recently been proposed  
121 (Yang et al., 2020) suggesting the potential for wide application if proxies based on 3-

122 OH-FA are available. Because Gram-negative bacteria are ubiquitous, 3-OH-FAs  
123 proxies could be applied to diverse archives, providing cross-correlation between  
124 speleothems (Wang et al., 2018), lake sediments, palaeosols and marine records (Yang  
125 et al., 2020). Proxies that span this environmental range are essential for elucidating  
126 links between marine and terrestrial climate change.

127 Even though the wide environmental occurrence of 3-OH-FAs has been known  
128 for some time, the development of 3-OH-FA based independent terrestrial  
129 environmental proxies was only recently initiated by Wang et al. (2016). Specifically,  
130 two temperature proxies, the ratio of *anteiso* to *normal* C<sub>15</sub> 3-OH-FA (RAN<sub>15</sub>, see Fig.  
131 1 for example structures) and the ratio of *anteiso* to *normal* C<sub>17</sub> 3-OH-FA (RAN<sub>17</sub>),  
132 were proposed as novel and independent temperature proxies (Wang et al., 2016).  
133 Several pH proxies, such as the ratio of the total sum of *iso* and *anteiso* 3-OH-FAs to  
134 the total amount of *normal* 3-OH-FAs (Branching Ratio) and the negative logarithm of  
135 Branching Ratio (RIAN), were proposed as novel pH proxies (Wang et al., 2016). The  
136 3-OH-FA based proxies for temperature (RAN<sub>15</sub>) and pH proxy (RIAN) were  
137 successfully applied to a stalagmite to produce the first biomarker based temperature  
138 and hydrological reconstructions from a speleothem archive (Wang et al., 2018).  
139 Studies of 3-OH-FAs from two altitudinal transects have confirmed the promise of  
140 these temperature and pH proxies (Huguet et al., 2019). Initial calibrations were limited  
141 to altitudinal soil transects from Mt. Shennongjia (central China), Mt. Rungwe (SW  
142 Tanzania) and Mt. Majella (central Italy), with a limited number of samples (Huguet et  
143 al., 2019; Wang et al., 2016). Recent work on additional altitudinal transects in Italy,  
144 Tibet and the Andes expands the number of sites investigated globally (Véquaud et al.,  
145 2020). Strong linear relationships between 3-OH FA-derived indices (RAN<sub>15</sub>, RAN<sub>17</sub>  
146 and RIAN) and MAAT/pH were obtained locally, but also highlighted variation in

147 calibration slopes and intercepts between discreet altitudinal transects (Véquaud et al.,  
148 2020). Another recent study from the French Alps found a high degree of scatter in the  
149 relationship between  $RAN_{15/17}$  and MAAT and taken together with the relatively weak  
150 relationships found on Mt. Majella suggests the relative abundance of these lipids  
151 maybe influenced by factors other than temperature and pH (Véquaud et al., 2020).  
152 Thus investigation based on a globally distributed soil sample set, including lowland  
153 samples and samples distributed at continental scales is needed to further explore the  
154 widespread applicability and constraint the accuracy of 3-OH-FA based proxies.

155 Here we aim to improve the accuracy and representativeness of the 3-OH-FA  
156 based proxies, extending the sample set of Wang et al. (2016) by adding 112 new  
157 surface soil samples globally located, and combining recently reported 3-OH-FAs  
158 distributions in soils from central China (Wang et al., 2018), NW Tanzania and central  
159 Italy (Huguet et al., 2019). The updated dataset confirms the first-order physiological  
160 response of Gram-negative bacterial membrane lipids to environmental drivers, but also  
161 finds significant differences in slopes and incepts of correlations and regional scales.  
162 Suggesting 3-OH-FA based proxies have great potential for widespread environmental  
163 applications, but that regional/ local calibrations and context will likely be required.

164

## 165 **2. Materials and methods**

### 166 **2.1 Soil sample collection and compilation**

167 Surface soils (0-10cm) used for this study are predominantly obtained from the soil  
168 sample repository of the International Soil Reference and Information Centre (ISRIC)  
169 in Wageningen, Netherlands, and from China and US. We obtained as many samples  
170 as possible (83) from the ISRIC repository that were previously studied for GDGT



171 analysis by Weijers et al. (2007), Peterse et al. (2012) and De Jonge et al. (2014), and  
172 from China which GDGT analysis were conducted previously by Yang et al. (2014)  
173 and Lei et al. (2016). In addition to the samples previously studied by Weijers et al.,  
174 2007 (and others), we collected a number of new samples in the field. The final sample  
175 dataset is composed of 186 globally distributed surface soils (Figs. 2 and  
176 S1;Supplementary Data), with 112 soil samples analysed for 3-OH-FAs in this study  
177 and 26 soil samples reported by Wang et al. (2016), 9 soil samples reported by Wang  
178 et al. (2018) and 39 soil samples reported by Huguet et al. (2019). The MAAT for the  
179 soil sampling sites ranged from -0.4 to 27°C. The soil pH of all soil samples ranged  
180 from 3.60 to 9.20.

## 181 **2.2 Determination of environmental parameters**

182 If available, soil pH data either comes from Weijers et al. (2007) (which is  
183 originally obtained from the ISRIC Soil Information System database), Yang et al.  
184 (2014), Lei et al. (2016) and Huguet et al. (2019). The pH of the remaining soils were  
185 measured following the method of Yang et al. (2014), specifically, soil samples were  
186 mixed with ultrapure water in a ratio of 1:2.5 (g/mL). After standing for 30 min, the  
187 supernatant pH was measured, using a pH meter with a precision of  $\pm 0.01$ . The pH was  
188 measured three times and the mean value was taken as the final pH.

189 The mean annual air temperature (MAAT) and mean annual precipitation (MAP)  
190 are from meteorological stations nearest to the sample locations. The climatic data for  
191 soil samples from ISRIC represents a 30-year average over the period 1961–1990  
192 (Weijers et al., 2007), for the soil samples from the US a 20-year average over the  
193 period of 1998 to 2017, for the rest of the soil samples a 30-year average over the period

194 1970-2000. If necessary, a temperature correction was performed for differences in  
195 altitude between the sample location and the weather station.

196

### 197 **2.3 Extraction of 3-OH-FAs**

198 The soil samples were freeze dried and ground with a mortar and pestle prior to  
199 extraction. The samples were subjected to acid hydrolysis following an optimized acid  
200 digestion method (Blyth et al., 2006; Wang et al., 2012). 10g of homogenized sample  
201 was mixed with 30 mL pre-cleaned HCl (3M), and then refluxed at 130 °C for 3h. After  
202 cooling, the solution was extracted x3 with DCM, to yield the Total Lipid Extract (TLE).  
203 The TLE was methylated by BF<sub>3</sub>-MeOH solution at 70 °C for 1.5h. The resulting fatty  
204 acid methyl esters (FAMES) were separated into non-OH-FAMES and OH-FAMES by  
205 silica gel column following the method described by Jenske and Vetter (2008). Non-  
206 OH-FAMES were eluted in the first fraction with a solvent mixture of *n*-hexane and  
207 ethyl acetate (v:v, 98:2), whereas OH-FAMES were obtained by elution with 100%  
208 ethyl acetate. The OH-FAME fraction was further derivatised by BSTFA (N, O-bis  
209 (trimethylsilyl) trifluoroacetamide) at 70 °C for 1.5 h before further analysis by gas  
210 chromatogram-mass spectrometer (GC-MS).

211

### 212 **2.4 GC-MS analysis of 3-OH-FAs**

213 The 3-OH-FAs were analysed by an Agilent 7890A gas chromatogram and 5975C  
214 mass spectrometer (GC-MS) equipped with a DB-5MS fused silica capillary column  
215 (60 m × 0.25 mm × 0.25 μm). The GC oven temperature was ramped from 70 °C to  
216 200 °C at 10 °C /min, then to 310 °C at 3 °C /min, held at 310 °C for 30 min. The carrier  
217 gas was Helium (99.999%) and the gas flow was 1.0 mL/min. The ionization energy of

218 the mass spectrometer was set at 70 eV. The 3-OH-FAs were identified based on their  
219 mass spectra and relative retention times, 3-OH-FA isomers with same carbon number  
220 come out in order of *iso*, *anteiso* and *normal* (Fig. 3). All the 3-OH-FAs TMSi esters  
221 show diagnostic fragment ions,  $m/z$  175 ( $[\text{CH}_3]_3\text{SiO}=\text{CHCH}_2\text{CO}_2\text{CH}_3^+$ ), due to the  
222 cleavage between  $\text{C}_3$  and  $\text{C}_4$ , and  $\text{M}^+-15$  (base peak) results from a loss of a  $\text{CH}_3$  group.  
223 Other characteristic ions include  $m/z$  103, 89, 133, 159, and  $\text{M}^+-31$  (Eglinton et al.,  
224 1968; Mielniczuk et al., 1993; Volkman et al., 1999; Wang et al., 2016).

225

## 226 **2.5 3-OH-FA based indices and mathematical analysis**

### 227 **2.5.1 Calculation of 3-OH-FA based indices**

228 3-OH-FA based indices, in particular the  $\text{RAN}_{15}$ ,  $\text{RAN}_{17}$  and  $\text{RIAN}$ , were  
229 calculated using the following equations, which were previously developed by Wang  
230 et al. (2016):

$$231 \text{RAN}_{15} = a\text{-C}_{15} / n\text{-C}_{15} \text{ 3-OH-FA} \quad (1)$$

$$232 \text{RAN}_{17} = a\text{-C}_{17} / n\text{-C}_{17} \text{ 3-OH-FA} \quad (2)$$

233 Where *a*- represents the *anteiso* homologue of 3-OH-FA, *n*- represents the *normal*  
234 homologue of 3-OH-FA.

$$235 \text{RIAN} = -\log ((I + A)/N) \quad (3)$$

236 Where *I* represents the sum of all the *iso* 3-OH-FAs, *A* represents the sum of all the  
237 *anteiso* 3-OH-FAs, and *N* represents the sum of all the *normal* 3-OH-FAs. Only 3-OH-  
238 FAs with carbon number range from  $\text{C}_{10}$  to  $\text{C}_{18}$  (derived from Gram-negative bacteria)  
239 were involved in the calculations. For the calibration of the other 3-OH-FAs based pH  
240 proxies, please refer to the Supplementary Information.

241 Analytical error bars are based on a) 14% of the soil samples being extracted and  
242 processed in duplicate or triplicate, e.g. ‘process duplicates’ and the average s.d. being  
243 applied to the samples that were not processed in duplicate (for this study, Wang et al.,  
244 2016, 2018), or b) triplicate injections e.g. Huguet et al., 2019. Errors for this study  
245 were 0.03 for RIAN, 0.29 for RAN<sub>15</sub> and 0.10 for RAN<sub>17</sub>. Errors for samples from  
246 Huguet et al., (2019) data were 0.006 for RIAN, 0.18 for RAN<sub>15</sub> and 0.05 for RAN<sub>17</sub>.  
247 The process duplicate errors are somewhat higher than the injection triplicates as would  
248 be expected. E.g. the process duplicates include variability from the entire process  
249 (extraction, column chromatography) as well as the GC-MS analysis.

250

### 251 **2.5.2 Statistical analysis**

252 We used the Canoco and Origin software to conduct the statistical analysis.  
253 Canoco 5 software was employed to determine the relationship of the fractional  
254 abundance of 3-OH-FAs and 3-OH-FA based indices to environmental factors. Firstly,  
255 a detrended correspondence analysis (DCA) was conducted to assess which model  
256 (linear or unimodal) was better suited to our dataset based on the length of gradient. If  
257 the length of gradient is below 2, a linear model analysis is suggested, while the length  
258 of gradient is above 2, a unimodal is suggested. The input data should be centered and  
259 standardised for linear model analysis. RDA, a type of linear model analysis, is a  
260 multivariate analogue of regression, and can be used to test the relationship of the 3-  
261 OH-FAs with one or more explanatory variables (in this case MAAT, pH, MAP and  
262 altitude).

263 Origin 2018 software was applied to test the Pearson correlation coefficient among  
264 the 3-OH-FA based indices (and their residuals) and environmental parameters.

265

### 266 **2.5.3 Machine Learning**

267 We used a Gaussian process (GP) emulator to make predictions for the  
268 environmental temperature and pH (outputs) based on the 3-OH-FA (input) data. A  
269 Gaussian process emulator is a machine learning tool that weighs a set of observations  
270 with known outputs (calibration data) in order to make predictions. The weights  
271 themselves are learned from the calibration. Typically, the GP will give greater weight  
272 to closer points in the input space. The training step thus consists of learning the  
273 appropriate distance metric on the multi-dimensional input space. A GP is able to  
274 handle high-dimensional inputs and find the best combinations, which allows for non-  
275 linear dependencies. It also provides quantified uncertainties on the output predictions  
276 (for technical details on GP regression refer to Rasmussen and Nickisch (2010) and  
277 Rasmussen and Williams (2006)). Our approach in applying GP regression to palaeo-  
278 proxy calibration builds on work by Dunkley Jones et al. (2020) who explore in detail  
279 the advantages of this approach versus pre-existing methods. Only samples with  
280 detectable quantities for all 3-OH-FA homologues (from C<sub>10</sub> to C<sub>18</sub>) were analysed for  
281 machine learning – resulting in a sample set of 158 (rather than 186). See [Section 5](#) for  
282 results and further discussion.

283 Model code and introduction for the calculation of  $D_{\text{nearest}}$  values and OPT3MAL  
284 MAAT and pH estimates (MATLAB script) are available at  
285 <https://github.com/carbonatefan/OPT3MAL>. MAAT and pH can be predicted using the  
286 full global (or a regional) data-set provided here or with any use defined data-set of 3-  
287 OH-FA fractional abundances (e.g. future regional or global datasets). The code is also  
288 archived in the [Zenodo repository https://doi.org/xxxxxxx](https://doi.org/xxxxxxx).

289

## 290 **3. Results**

### 291 **3.1 Composition and Distribution of 3-OH-FAs in soil samples**

292 Data from a total of 186 globally distributed surface soil samples were compiled,  
293 including new 112 soil samples analysed in this study (see Section 2.1). The complete  
294 results for each sample are provided in the [Supplementary Data](#). The MAAT for the  
295 soil sampling sites ranged from -0.4 to 27.0°C ([Fig. 2](#)). The soil pH of all soil samples  
296 ranged from 3.60 to 9.20 (see [Fig. 7](#)). The range of pH is extended by 2 pH units (ca. 1  
297 pH unit at both ends of the spectrum) compared to previously reported data sets (Huguet  
298 et al., 2019; Wang et al., 2016). The MAP ranged from 374 to 3313 mm ([Supplementary](#)  
299 [Data](#)).

300 The molecular fingerprint of 3-OH-FAs in soil samples is akin to that derived from  
301 the LPS component of the outer membrane of Gram-negative bacteria (Klok et al., 1988;  
302 Lee et al., 2004; Tyagi et al., 2015; Wakeham et al., 2003; Wang et al., 2018). 3-OH-  
303 FAs were present in every soil sample analysed, supporting earlier studies on the  
304 widespread occurrence of 3-OH-FAs in widely distributed altitudinal transects ([Huguet,](#)  
305 [et al., 2019, Wang, et al., 2016](#)) and suggesting a ubiquitous distribution of these  
306 membrane lipids in soils. Thus we assume that the 3-OH-FAs measured in the soils  
307 originate from the soil dwelling consortia of Gram-negative bacteria (Wang et al., 2016).

308 Large differences in the relative concentration of different 3-OH-FA homologues  
309 occurred throughout the sample set, displaying distinctive changes in chemical  
310 homologue distributions along environmental gradients ([Figs. 2&3; S1& S2](#)). The  
311 carbon number of 3-OH-FAs ranged from C<sub>10</sub> to C<sub>18</sub>, including *iso* C<sub>11</sub>, C<sub>12</sub>, C<sub>13</sub>, C<sub>14</sub>,  
312 C<sub>15</sub>, C<sub>16</sub>, C<sub>17</sub>, C<sub>18</sub> and *anteiso* C<sub>11</sub>, C<sub>13</sub>, C<sub>15</sub>, C<sub>17</sub> 3-OH-FAs, with the *normal* C<sub>12</sub>, C<sub>14</sub>,

313 C<sub>16</sub> and C<sub>18</sub> homologues being typically most abundant (Fig. 3). The summed *normal*  
314 3-OH-FAs are the most abundant, followed by the *iso* 3-OH-FAs, then the *anteiso* 3-  
315 OH-FAs. Observations apparent from the chromatograms are the visible differences in  
316 distribution in the dominant 3-OH-FA homologue, and the relative abundance of the  
317 *normal* vs *iso* and *anteiso* isomers in the different soil samples (Figs. 2&3; S1& S2).  
318 Especially apparent is the relative increase in the *anteiso* isomers of the C<sub>15</sub> and C<sub>17</sub>  
319 homologues in soil samples with colder MAATs (Figs. 2 & S2).

320 The dominant compound in the global soil samples is the *normal* C<sub>14</sub> (155 out of  
321 186). In the other samples, the dominant compound is either the *normal* C<sub>12</sub>, C<sub>16</sub>, C<sub>18</sub>  
322 or *iso* C<sub>17</sub>. Similar variations in the predominant compounds were reported in soils by  
323 Wang et al. (2016), Huguet et al. (2019) and Véquaud et al. (2020), and in snow pit  
324 samples reported by Tyagi et al. (2016). Laboratory culture experiments show that the  
325 dominant compounds varied among C<sub>10</sub>, C<sub>12</sub>, C<sub>14</sub>, C<sub>16</sub> within different Gram-negative  
326 genera and species (Goossens et al., 1986; Hedrick et al., 2009; Oyaizu and Komagata,  
327 1983). For example, species of Gammaproteobacteria such as *Pseudomonas* appear to  
328 produce mainly even carbon numbered 3-OH-FAs, particularly C<sub>10</sub>, C<sub>12</sub> and C<sub>14</sub>  
329 (Humphreys et al., 1972; Ikemoto et al., 1978; Oyaizu and Komagata, 1983; Wilkinson  
330 et al., 1973; Wollenweber et al., 1984). A large number of species in the phylum  
331 Bacteroidetes seem to have a dominance of C<sub>15</sub>, C<sub>16</sub> and C<sub>17</sub>, compounds not commonly  
332 identified in Gammaproteobacteria (Bernardet et al., 1996; Lee et al., 2007; Miyagawa  
333 et al., 1979; Wollenweber et al., 1980). Thus the changes of the dominant compound in  
334 soil samples (and regional differences in RAN<sub>15/17</sub> and RIAN calibration slopes and  
335 intercepts) may be due to the variation of Gram-negative bacterial community  
336 composition. However, we found no systematic variation of the predominant compound  
337 with changes in environmental parameters. Future study on the Gram-negative bacteria

338 community composition of soils using genomic methods in representative soil samples  
339 will give insights into this. Furthermore, a comprehensive evaluation of the 3-OH-FA  
340 compounds produced by a wide diversity of Gram-negative bacteria is required to  
341 identify the main producers of 3-OH-FAs in different environments as previous  
342 research focuses on more readily culturable species of Gammaproteobacteria, and  
343 reports on the 3-OH-FA composition for phyla such as Acidobacteria, Chloroflexi,  
344 Planctomycetes and Verrucomicrobia appear to be much more limited.

345

### 346 **3.2 Correlation of 3-OH-FA based indices and environmental proxies**

347 Below we explore correlations of previously published 3-OH-FA based proxies to  
348 environmental parameters in the new global soil compilation dataset.  $RAN_{15}$  ranged  
349 from 0.54 to 10.18,  $RAN_{17}$  ranged from 0.26 to 4.75. Within the MAAT range of this  
350 study (-0.4 to 27°C), both the  $RAN_{15}$  and  $RAN_{17}$  showed negative linear correlations  
351 with MAAT ( $r = -0.69$ ,  $p < 0.001$  and  $r = -0.64$ ,  $p < 0.001$ , respectively) (Figs. 4 and 5).  
352 The 3-OH-FAs based pH proxies, including the Branching Ratio, RIAN, Branched  
353 Index and RIN, were calculated for all the soil samples. Here, in the main text, we focus  
354 on the RIAN proxy but we present the results of the other pH proxies in the  
355 [Supplementary Information](#). The RIAN index ranges from 0.11 to 0.98 with soil pH  
356 ranging between 3.60 and 9.20 and shows a negative linear correlation with the soil pH  
357 ( $r = -0.81$ ,  $p < 0.001$ ) (Figs. 4 and 5).

358 Statistical analyses were performed using Canoco software to explore the impacts  
359 of environmental parameters on the distribution of 3-OH-FAs and 3-OH-FAs based  
360 indices (See [Supplementary Section 2](#)). The DCA analysis revealed that a linear model  
361 was more appropriate for our dataset as the length of gradient is less than 2, then



362 redundancy analysis (RDA) was performed. The RDA results confirm that soil pH and  
363 MAAT are the dominant controls on the distribution of 3-OH-FAs, while the other two  
364 environmental parameters, MAP and altitude, show insignificant effects on the  
365 distribution of 3-OH-FAs (Table S1 and Fig. S4A). Soil pH explains 24% of the  
366 variation of the 3-OH-FAs distribution and MAAT explains 5.8% (Table S1). Soil pH,  
367 MAAT and MAP are the dominant controls on the 3-OH-FA based indices (Table S2  
368 and Fig. S4B). Soil pH explains 45.6% variation of 3-OH-FA based indices and MAAT  
369 explains 12.4% (Table S2). Further exploration of the data using machine learning was  
370 conducted and is discussed in section 5.

## 371 4. Discussion

### 372 4.1 Effect of temperature on the distribution of 3-OH-FAs

373 In our global soil compilation,  $RAN_{15}$  and  $RAN_{17}$  vary from 0.54 to 10.18 and  
374 0.26 to 4.75 respectively, covering greater cumulative ranges than reported previously  
375 for initial altitudinal transect studies (Huguet et al., 2019; Wang et al., 2016;  
376 Supplementary Datasheet). In our global calibration,  $RAN_{15}$  shows a significant linear  
377 relationship with MAAT ranging from -0.4 to 27.0 °C ( $r = -0.69$ ,  $p < 0.001$ ; Fig. 4),  
378  $RAN_{17}$  shows a linear correlation with MAAT as well but the correlation coefficient is  
379 relatively lower ( $r = -0.64$ ,  $p < 0.001$ ; Fig. 4).

380 Based on the global soil calibration, the updated MAAT equations based on  $RAN_{15}$   
381 and  $RAN_{17}$  are (Fig. 5):

$$382 \text{ MAAT} = 36.29 - 5.88 \times \text{RAN}_{15} \quad (n = 186, R^2 = 0.47, p < 0.001, \text{RMSE} = 4.9 \text{ } ^\circ\text{C}) \quad (4)$$

$$383 \text{ MAAT} = 37.68 - 14.49 \times \text{RAN}_{17} \quad (n = 185, R^2 = 0.39, p < 0.001, \text{RMSE} = 5.2 \text{ } ^\circ\text{C}) \quad (5)$$

384 The above equations show that MAAT has a significant effect on the distribution  
385 of C<sub>15</sub> and C<sub>17</sub> 3-OH-FAs in the globally distributed soil samples. Both RAN<sub>15</sub> and  
386 RAN<sub>17</sub> increased with decreasing temperature. This is supported by the general  
387 principle of membrane adaptation to temperature, such that bacteria increase the  
388 proportion of *anteiso* 3-OH-FAs (increasing the RAN indices) with decreasing  
389 temperature in order to maintain membrane fluidity (see inset boxes in Fig. 2). *Anteiso*  
390 fatty acids have a lower melting point than *normal* and *iso* fatty acids (Kaneda, 1991;  
391 Suutari and Laakso, 1994). Specifically, Kaneda (1991) found that the melting point of  
392 the *a*-C<sub>15</sub> (23.0°C) and *a*-C<sub>17</sub> (36.8°C) fatty acids were 29.5°C and 24.5°C lower than  
393 the melting points of the *n*-C<sub>15</sub> (52.5°C) and *n*-C<sub>17</sub> (61.3°C) fatty acids, respectively.  
394 Phase transition temperature is even more closely related to membrane fluidity than the  
395 average melting temperature of compounds (Kaneda, 1991) and is defined as the  
396 temperature required to induce a change in the lipid physical state from the ordered gel  
397 phase, where the hydrocarbon chains are fully extended and closely packed, to the  
398 disordered liquid crystalline phase, where the hydrocarbon chains are randomly  
399 oriented and fluid. Kaneda (1991) found the phase transition temperature for the *a*-C<sub>15</sub>  
400 (-16.5°C) and *a*-C<sub>17</sub> (7.6°C) were 50.7°C and 41.2°C lower than the equivalent points  
401 for the *n*-C<sub>15</sub> (34.2°C) and *n*-C<sub>17</sub> (48.8°C). Furthermore, the *anteiso*-positioned fatty  
402 acids have a greater disturbance of the packing order of the hydrocarbon chains (Russell,  
403 1995). All of these changes may contribute to maintaining permeability and a liquid  
404 crystalline phase of the plasma membrane at different environmental temperatures  
405 (Koga, 2012; Siliakus et al., 2017).

406 It is worth noting that, as well as having a slightly higher R<sup>2</sup> value (and lower  
407 RMSE), the RAN<sub>15</sub> index undergoes a greater absolute change in index value (0.54 to  
408 10.18) compared to RAN<sub>17</sub> (0.26 to 4.75). This indicates a fundamentally higher

409 amplitude response in the distribution of the C<sub>15</sub> 3-OH-FA homologues compared to  
410 the C<sub>17</sub> 3-OH-FA homologues along our global MAAT gradient and is illustrated by  
411 comparing Figs. 2 and S2. E.g. the proportional increase in relative abundance of *a*-C<sub>15</sub>  
412 vs *n*-C<sub>15</sub> produced at colder temperatures is ca. double that of the increase in *a*-C<sub>17</sub> vs  
413 *n*-C<sub>17</sub>. This may be due to the larger variation range and relatively higher abundances  
414 of *a*-C<sub>15</sub> 3-OH-FA in our global soil samples (Fig. S3). This apparently greater physio-  
415 chemical response of the C<sub>15</sub> 3-OH-FA homologues would appear to recommend  
416 RAN<sub>15</sub> as a potentially better palaeo-temperature proxy over RAN<sub>17</sub>. Moreover, the  
417 residuals of RAN<sub>15</sub> showed no correlation with pH or precipitation which shows the  
418 residuals or RAN<sub>15</sub> are truly random (Supplementary Fig. S9). However, we note that  
419 RAN<sub>15</sub> has relatively more scatter than the RAN<sub>17</sub> proxy when MAAT is below 10 °C,  
420 possibly indicating that RAN<sub>17</sub> may be more suitable for low temperature  
421 reconstructions. Further study including genomic analyses, insights to bacterial  
422 producer populations and culture experiments are required to confirm this.

423 We note that at a global scale, the relationship between RAN<sub>15</sub>/RAN<sub>17</sub> and MAAT  
424 contains significant scatter, likely highlighting how other environmental parameters,  
425 bacterial biogeography and physical soil effects may affect the variation of the  
426 RAN<sub>15</sub>/RAN<sub>17</sub> proxies. For instance, we take the recent 30-year average air temperature  
427 as representative of the soil temperature, which may be not accurate. This is due to the  
428 inherently heterogenous nature of soils, whereby near surface soil conditions and  
429 temperatures which bacteria experience may be offset from the boundary layer MAAT  
430 estimated from interpolating weather station data. This offset between soil and air  
431 temperatures is also not constant, varying with changes of vegetation type, vegetation  
432 coverage, soil moisture and texture, etc. (Chudinova et al., 2006; Wang et al., 2020)..  
433 Furthermore, the weak anticorrelation between MAAT and soil pH ( $r = -0.34$ ,  $p < 0.05$ ;

434 Fig. 4) may add scatter to the correlation between 3-OH-FA based temperature proxies  
435 and MAAT. However, we notice that the correlation coefficients of 3-OH-FA based  
436 temperature proxies with pH ( $r = 0.15$ ,  $p < 0.05$  and  $0.34$ ,  $p < 0.05$ , respectively) are  
437 much lower than those with the MAAT ( $r = -0.69$ ,  $p < 0.001$  and  $r = -0.64$ ,  $p < 0.001$ ,  
438 respectively; Fig. 4). As discussed in the next section, pH is the dominant  
439 environmental control on bacterial biogeographies at regional scales (Griffiths et al.,  
440 2011). Shifting bacterial compositions may in turn affect the distribution of 3-OH-FAs  
441 in soils, as some bacterial taxa with distinctive 3-OH-FA signatures may dominate in a  
442 particular region (Goossens et al., 1986; Hedrick et al., 2009; Oyaizu and Komagata,  
443 1983). We note that a recent re-evaluation of GDGT based temperature and pH proxies  
444 in global soils shows that soil type may bias MAAT and pH estimates (Davtian et al.,  
445 2016) and that vegetation cover in the sample site may also influence the community  
446 structure of the Gram-negative bacteria, as Gram-negative bacteria prefer to utilise  
447 more plant-derived C sources that are relatively labile (Fanin et al., 2019). The  
448 combinations of environmental factors driving bacterial community structure are  
449 complex, and the major determinants may be region and taxa-specific (Oliverio et al.,  
450 2017; Singh et al., 2013; Yao et al., 2017). Both these effects will require further study  
451 in the development of 3-OH-FA based proxies.

452 Because of the scatter in the global calibration we investigated the correlations for  
453  $RAN_{15}$  and  $RAN_{17}$  for discrete regions (Fig 6). We find that for the  $RAN_{15}$  and  $RAN_{17}$   
454 temperature proxies there are significant differences in slope and intercept of the linear  
455 corrections at regional scales. The coefficient of determinations between  $RAN_{15}$  and  
456 MAAT varied from 0.30 to 0.79 in regional calibrations (Fig. 6A, Supplementary Data).  
457 The strongest correlation between  $RAN_{15}$  and MAAT were observed in Mount Rungwe  
458 ( $R^2 = 0.79$ ,  $p < 0.001$ ), strong correlation was also found in Northern America ( $R^2 = 0.74$ ,

459  $p < 0.001$ ). Moderate correlations were observed in Mount Shennongjia, Mount Majella  
460 and Africa & Europe ( $R^2 = 0.50$ ,  $p < 0.001$ ,  $R^2 = 0.44$ ,  $p < 0.05$ ,  $R^2 = 0.49$ ,  $p < 0.001$ ,  
461 respectively). The samples from China had the most scatter ( $R^2 = 0.30$ ,  $p < 0.001$ ). For  
462 the  $RAN_{17}$  proxy, the coefficient of determinations varied from 0.28 to 0.74 in regional  
463 calibrations, except the Mount Majella and Africa & Europe where no significant  
464 correlations were found (Fig. 6B, Supplementary Data). The strongest correlation  
465 between  $RAN_{17}$  and MAAT were observed in Northern America ( $R^2 = 0.74$ ,  $p < 0.001$ ),  
466 moderate to weak correlations were observed in Mount Rungwe, Mount Shennongjia  
467 and China ( $R^2 = 0.48$ ,  $p < 0.001$ ,  $R^2 = 0.52$ ,  $p < 0.001$ ,  $R^2 = 0.28$ ,  $p < 0.001$ , respectively).  
468 The lack of correlation in Africa & Europe may be due to the  $RAN_{17}$  being relatively  
469 less sensitive to temperature changes when MAAT is above 20 °C; a similar feature is  
470 also found in brGDGT based  $MBT'_{5ME}$  proxy (De Jonge et al., 2014; Naafs et al., 2017).  
471 Thus local or regional calibrations are likely preferable (at this stage of 3-OH-FA proxy  
472 development) for application to palaeoclimate archives. For example, applying our  
473 global linear calibration to the only available 3-OH-FA based palaeo-record from a  
474 Chinese speleothem would result in a large overestimation of temperature (compared  
475 to the existing local calibration used by Wang et al., 2018).

476

#### 477 **4.2 Effect of pH on the distribution of 3-OH-FAs**

478 pH is an important environmental parameter which affects the soil bacterial  
479 community structure and diversity (Bååth and Anderson, 2003; Delgado-Baquerizo et  
480 al., 2018; Griffiths et al., 2011; Lauber et al., 2009; Rousk et al., 2010). Acidic soils  
481 have commonly been found to support a lower diversity of bacteria, with a dominance  
482 of low pH specialists such as Acidobacteria in soils with a pH below 5 (Cho et al., 2019;

483 Jones et al., 2009; Lauber et al., 2009; Zhang et al., 2015). More importantly, pH can  
484 influence membrane fluidity, and lead to the changes in membrane lipids (Wang et al.,  
485 2016). For example, culture experiments on a strain of Gram-negative bacteria showed  
486 increased/decreased relative abundance of branched-chain fatty acids in higher  
487 pH/lower pH (Giotis et al., 2007). Our results from the global soil samples indicate that  
488 the proportion of Gram-negative bacteria derived branched 3-OH-FA homologues is  
489 affected by soil pH. These are illustrated by the correlations between the 3-OH-FA  
490 based indices and soil pH (Fig. 7 & S5).

491 In accordance with previous findings (Wang et al., 2016), the Branching Ratio  
492 showed an exponential relationship with soil pH (Fig. S5A). Since soil pH has a  
493 logarithmic relationship with the concentration of H<sup>+</sup>, this suggests the variation of the  
494 Branching Ratio may be influenced by the concentration of soil H<sup>+</sup>. Lower pH  
495 corresponds to a larger concentration of H<sup>+</sup>, and thus steeper proton gradients across  
496 bacterial cell membranes. We suggest that the observation of a decreasing Branching  
497 Ratio at lower pH reflects chemiosmotic coupling, i.e., the production of fewer  
498 branched homologues, producing a less fluid or more impermeable membrane to  
499 counteract steeper proton gradients (Denich et al., 2003; McElhaney et al., 1973;  
500 Russell and Fukunaga, 1990). The existence and maintenance of a proton gradient over  
501 bacterial cell membranes is vital for the energy supply of a cell (Mitchell, 1966) and  
502 involves the trapping of proton-conducting water molecules in the lipid core of the  
503 membranes (Nagle and Morowitz, 1978; Wikström et al., 2015). Given the logarithmic  
504 relationship between pH and the Branching Ratio (Fig. S5A) and the definition of pH  
505 as the negative logarithm of the proton concentration, it is possible to obtain a linear  
506 relationship between the two by using the previously defined RIAN index:

$$507 \quad \text{RIAN} = -\log (\text{Branching Ratio}) \quad (6)$$

508 The linear relationship between the RIAN and global soil pH is best fit by:

$$509 \text{ RIAN} = 1.12 - 0.11 \times \text{pH} \quad (n = 186, R^2 = 0.66, p < 0.001, \text{RMSE} = 0.10) \quad (7)$$

510 This relationship between the RIAN index and soil pH is similar to what was  
511 previously reported (Huguet et al., 2019; Wang et al., 2016). The global calibration is  
512 consistent with previous local/regional calibration suggesting a wider applicability of  
513 the proxy in global soil samples. This is consistent with previous research on bacterial  
514 brGDGTs indicating that soil pH has a significant impact on the global soil brGDGTs  
515 distribution (Peterse et al., 2012; Weijers et al., 2007; Yang et al., 2012).

516 Based on the above correlation, we propose new global transfer equation for soil  
517 pH calibration:

$$518 \text{pH} = 10.18 - 9.09 \times \text{RIAN} \quad (n = 186, R^2 = 0.66, p < 0.001, \text{RMSE} = 0.78) \quad (8)$$

519 The pH proxies developed by Wang et al. (2016) were only based on 26 soil  
520 samples along an altitudinal transect of Mt. Shennongjia. In this paper, we have used  
521 186 globally located soil samples, which greatly extended sample size and locations.  
522 Moreover, the pH range in our updated calibration ranges from 3.60 to 9.20,  
523 significantly extending the pH range compared to previous calibrations (Fig. 7), further  
524 confirming the applicability of RIAN (and other 3-OH-FA based indices) as a novel pH  
525 proxy.

526 Regional calibrations were also conducted to test the consistency of global and  
527 regional calibrations (Fig. 8). The results showed that samples from China, Northern  
528 America and Mt. Shennongjia shared identical slopes and intercepts with the global  
529 calibration. But samples from Mount Rungwe showed no significant correlation  
530 between RIAN and soil pH, this may be due to the narrowed pH changes in that region  
531 (Huguet et al., 2019). Samples from Africa & Europe also showed no significant

532 correlations. Interestingly, a reversed correlation was found in Mount Majella ( $R^2 =$   
533  $0.65$ ,  $p < 0.05$ ) which is completely different from the other regional and global  
534 calibrations in this study (Fig. 8 and Supplementary Data). Thus regional calibration  
535 may be more appropriate in some site specific settings.

536

### 537 **4.3 Effect of precipitation on the distribution of 3-OH-FAs**

538 Mean Annual Precipitation (MAP) varies from 374 to 3313 mm in our global soil  
539 compilation, covering samples from semi-arid to tropical zones. Despite a generally  
540 observed relationship between effective precipitation and pH in global soils (Slessarev  
541 et al., 2016; Yang et al., 2014), MAP for our soil samples shows low correlation with  
542 pH ( $r = -0.47$ ,  $p < 0.001$ ; Figs. 4 and S6). In our global soil dataset, we found weak  
543 correlations between the MAP and 3-OH-FAs based proxies (Figs. 4 and S7). Weak  
544 correlation between MAP and 3-OH-FAs were also found in Mt. Majella (Huguet et al.,  
545 2019), but no correlation was found in the samples from our original study on Mt.  
546 Shennongjia (Wang et al., 2016). Notably, we found no correlations between MAP and  
547 soil pH in Mt. Shennongjia ( $r = -0.27$ ,  $p > 0.05$ ) (Wang et al., 2016) and weak  
548 correlation in the global soil dataset ( $r = -0.47$ ,  $p < 0.001$ ; Fig. 4 and S6). The weak  
549 correlation between the MAP and 3-OH-FAs based proxies in the global soil samples  
550 suggests that MAP may affect the community composition of Gram-negative bacteria,  
551 and thus the distribution of 3-OH-FAs, although this appears to be a secondary effect  
552 compared to pH. Manipulative experiments in different steppes along a precipitation  
553 gradient in northern China showed that precipitation regime controls microbial activity  
554 and biomass, possibly by regulating soil moisture and substrate availability (Liu et al.,  
555 2016). Metagenomics of global topsoil samples show that bacterial global niche



556 differentiation is associated with contrasting diversity responses to precipitation and  
557 soil pH (Bahram et al., 2018).

558 We found no linear correlations between precipitation and RAN<sub>15</sub>/RAN<sub>17</sub>, suggesting  
559 that precipitation likely does not affect the values of our 3-OH-FA based temperature  
560 proxies (Fig. S8). This independence of the 3-OH-FA based temperature proxies may  
561 be because only the *anteiso* and *normal* C<sub>15</sub> or C<sub>17</sub> homologues are utilised in these  
562 proxies. In comparison GDGT analysis of soil transects from the US highlights a  
563 substantial increase in the offset between measured MAAT and MBT/CBT-based  
564 MAAT below an annual precipitation of 700–800 mm yr<sup>-1</sup>, implying an impact of  
565 precipitation amount on MBT/CBT-based temperature reconstruction (possibly related  
566 to soil aeration and pH) (Dirghangi et al., 2013). The study of bacterial GDGTs  
567 (brGDGTs) from global surface soils samples shows the relative abundance of some  
568 brGDGTs, but not all correlate with MAP (De Jonge et al., 2014; Peterse et al., 2012;  
569 Weijers et al., 2007). Our observation that MAP shows some impact on 3-OH-FA based  
570 pH proxies (Branching Ratio:  $r = -0.51$ ,  $p < 0.001$ ; RIAN:  $r = 0.49$ ,  $p < 0.001$ ; Branched  
571 Index:  $r = -0.51$ ,  $p < 0.001$ ; RIN:  $r = -0.51$ ,  $p < 0.001$ ; Figs. 4 and S7), but no impact  
572 on 3-OH-FA based temperature proxies may reflect changes in bacterial community  
573 composition and diversity between different precipitation regimes. Our pH indices,  
574 including RIAN, incorporate up to 21 different 3-OH-FA homologues and thus are  
575 more likely to reflect an aggregate change of 3-OH-FAs resulting from any differences  
576 in Gram-negative bacteria community between higher and lower precipitation regime  
577 soils. Whereas the more limited use of only 2 different homologues in the RAN<sub>15</sub> and  
578 RAN<sub>17</sub> indices must be inherently more specific to particular classes of Gram-negative  
579 bacteria.

580

#### 581 **4.4 Comparison with GDGT data**

582 GDGT based proxies are well established for palaeoenvironmental reconstructions.  
583 In our new global dataset, MBT'<sub>5ME</sub>-MAAT shows linear correlations with RAN<sub>15</sub> and  
584 RAN<sub>17</sub> proxies, but the correlation coefficient is relatively low ( $r = -0.59$ ,  $p < 0.001$  and  
585  $r = -0.42$ ,  $p < 0.001$ , respectively; Fig. 9). The relatively low correlation between the 3-  
586 OH-FA based RAN<sub>15</sub>/ RAN<sub>17</sub> and GDGT based MBT'<sub>5ME</sub> may be partly due to the  
587 intrinsic relatively lower correlations between the 3-OH-FA based temperature proxies  
588 and MAAT, or due to different responses of Gram-negative bacteria and brGDGT-  
589 producing bacteria to other environmental factors (Huguet et al., 2019). Interestingly,  
590 the MBT'<sub>5ME</sub> data which are available for the samples in this study also showed different  
591 slopes and intercepts in global and regional calibrations (Fig. S10). This may add the  
592 scatter to the correlation of 3-OH-FA based RAN<sub>15</sub>/ RAN<sub>17</sub> and GDGT based MBT'<sub>5ME</sub>  
593 indices. The cyclisation ratio of branched tetraethers (CBT) is an established pH proxy,  
594 first proposed by Weijers et al. (2007). We find that our 3-OH-FA based pH proxies  
595 show significant correlation with CBT (Branching Ratio:  $r = -0.72$ ,  $p < 0.001$ ; RIAN:  $r$   
596  $= 0.77$ ,  $p < 0.001$ ; Branched Index:  $r = -0.75$ ,  $p < 0.001$ ; RIN:  $r = -0.70$ ,  $p < 0.001$ ; Fig.  
597 10), further confirming that these bacterial derived membrane lipids are both controlled  
598 by soil pH.

599

#### 600 **5. Further examination and calibration of relationships between 3-OH-FAs** 601 **distributions with MAAT and soil pH using machine learning**

602 The linear regression based indices above are defined by empirically linking  
603 environmental controls with a presumed, but unproven, physiological mechanism of

604 membrane adaptation by the soil bacteria producing the 3-OH-FAs, i.e. an increase in  
605 the percentage of *anteiso* isomers with decreasing MAATs, and an increase in the  
606 percentage of branched isomers with increasing pH. There are a number of options to  
607 improve predictions based on linear regressions using machine learning techniques  
608 such as artificial neural networks, random forests and Gaussian Process emulators.  
609 These flexible, non-parametric models are all based on the idea of training a predictor  
610 by fitting a set of coefficients in a sufficiently complex, often multi-layer, model in  
611 order to minimise residuals on the calibration data set (Fig. 11). The objective is to  
612 search, agnostically, among a large space of smoothly varying functions of 3-OH-FA  
613 compositions for those functions which adequately describe temperature and pH  
614 variability. This, essentially, is a way of combining information from all calibration  
615 data points, not just the nearest neighbours, assigning different weights to different  
616 calibration points depending on their utility in predicting the temperature or pH at the  
617 input of interest.

618 GP regressions were applied to both the full input range of 3-OH-FA homologues  
619 and to the subset of compounds, which have previously demonstrated the clearest  
620 sensitivity to MAAT (the *i*-C<sub>15</sub>, *a*-C<sub>15</sub>, *n*-C<sub>15</sub>, *i*-C<sub>17</sub>, *a*-C<sub>17</sub>, *n*-C<sub>17</sub> isomers as utilized in  
621 the RAN<sub>15</sub> and RAN<sub>17</sub> indices). 90% of data points were used for calibration. Validation  
622 and performance were tested using the remaining 10% of data points, repeating the  
623 process 10 times with a random choice of which data fall into the calibration (90%) and  
624 validation (10%) groups.

625 By using all data the GP regression approach gives superior results compared to  
626 the simple linear regressions (Section 4.1) for both temperature (Fig. 12A: RSME =  
627 3.5°C; R<sup>2</sup> = 0.66) and pH (Fig. 12B: RSME = 0.76 pH units; R<sup>2</sup> = 0.63). GP regression

628 provides a confidence interval on the prediction (see Fig. 12), which can be used to test  
629 the self-consistency of the prediction: for example, we expect that the true value should  
630 fall into the 90% confidence interval 90% of the time. When using all of the isomers  
631 from C<sub>10</sub> to C<sub>18</sub> the validation value is contained within the 5 to 95% confidence interval  
632 of GP predictions only 80% of the time for temperature and 77% of the time for pH,  
633 rather than the expected 90%. This indicates the possibility of a systematic bias, perhaps  
634 because the large dimensionality of the input data means that there is often no  
635 calibration data sufficiently nearby (in parameter space) and the model is forced to  
636 extrapolate instead of interpolating.

637 GP regression using just the C<sub>15</sub> and C<sub>17</sub> *iso*, *anteiso* and *normal* isomers yields  
638 superior results compared to the simple linear regressions for both temperature (Fig.  
639 12B: RSME = 3.9°C; R<sup>2</sup> = 0.61) and pH (Fig. 12C: RSME = 0.64 pH units; R<sup>2</sup> = 0.74).  
640 Moreover, unlike GP regression based on all isomers from C<sub>10</sub> to C<sub>18</sub>, when using only  
641 the C<sub>15</sub> and C<sub>17</sub> *iso*, *anteiso* and *normal* isomers, the validation values were contained  
642 within the 5 to 95% interval 93% of the time for temperature and 91% of the time for  
643 pH, statistically consistent with the expected 90%.

644 In addition to naturally yielding confidence limits on predictions, GP regression  
645 has the benefit of providing estimates of the relative importance of the inputs in  
646 predicting the output. By examining the learned GP kernel, we find that *anteiso* and  
647 *normal* C<sub>15</sub> and *iso* and *anteiso* C<sub>17</sub> play significant roles in temperature prediction,  
648 while *iso*, *anteiso* and *normal* C<sub>17</sub> isomers and *anteiso* C<sub>15</sub> play comparable roles in pH  
649 prediction.

650 In Fig.12 we illustrate the GP regressions for all the available global soils samples.  
651 But it should be noted that our code can be run on regional (or user defined) data-sets.

652 This may be desirable for specific applications, due to regional differences observed in  
653 the empirical linear regressions.

654 The superior performance of machine-learning on the sufficiently complex, multi-  
655 dimensional data set is not unexpected. It is able to effectively consider a much broader  
656 range of possible dependencies than those analysed in Section 4.1, including possible  
657 non-linear behaviour of the output as a function of inputs. Therefore, in the absence of  
658 a robust physical model, machine learning yields a preferred approach to making  
659 accurate predictions. It does suffer from an inability to extrapolate to input data regimes  
660 that are far from the available calibration data, though caution is always warranted for  
661 such extrapolation in the absence of a robust model (and if such a model does exist, it  
662 can be readily incorporated into the machine learning tools). The machine learning  
663 predictions are also challenging to translate into a human-readable model, though at  
664 least in the case of a GP emulator, the learned metric on the parameter space can be  
665 useful for interpreting which input parameters play the most significant roles in  
666 determining temperature and pH outputs. These limitations are generally more than  
667 compensated by increased prediction accuracy (e.g., Dunkley Jones et al., 2020), and  
668 by the availability of prediction uncertainties along with best-guess estimators.

669

## 670 **6. Conclusion**

671 Based on an extensive new global compilation ( $n = 186$ ), we tested the performance of  
672 3-OH-FA based proxies for MAAT and pH in global soil samples. We find that the 3-  
673 OH-FA based temperature proxies  $RAN_{15}$  and  $RAN_{17}$  show significant correlations  
674 with MAAT and the 3-OH-FA based pH proxy  $RIAN$  shows a significant correlation  
675 with soil pH. Machine learning based GP emulator models confirm that environmental

676 signals are recorded by 3-OH-FAs. Moreover, the GP regressions give higher  $R^2$  values  
677 and reduce RSME; they also provide confidence intervals on the predictions. We  
678 recommend that workers explore and apply both the simple linear regressions and  
679 machine-learning based models to palaeoclimate data-sets during this nascent stage of  
680 3-OH-FA development for palaeoclimate. Moreover, we find that for our 3-OH-FA  
681 based proxies there are significant differences in slope and intercept of the linear  
682 corrections at regional scales. Thus local or regional calibrations are likely preferable  
683 at this stage of 3-OH-FA proxy development for application to specific palaeoclimate  
684 archives. While this manuscript was under review, Véquaud et al. (2020) applied other  
685 machine learning tools, including random forests, to this problem, achieving broadly  
686 similar results. Our empirical, global scale, compilation of 3-OH-FA based proxies  
687 builds on the promise of initial altitudinal calibrations (and a Holocene stalagmite  
688 climate reconstruction) and has wide implications for palaeoclimatic and environmental  
689 studies. Gram-negative bacteria are ubiquitous in natural environments, and 3-OH-FA  
690 based proxies are now developed for both terrestrial and marine settings. These  
691 compounds are easy to extract using a simple acid digestion and to analyse using GC–  
692 MS and GC–FID systems. This makes it possible to obtain high-resolution palaeo-  
693 records using a relatively small sample mass. We hope this investigation open up new  
694 avenues of research on 3-OH-FAs, including culture studies and DNA sequencing to  
695 constrain 3-OH-FA bacterial precursors, to investigate the underlying response  
696 mechanisms to environmental parameters, and applications to an array of  
697 palaeoclimatic archives (e.g., palaeosols, lakes, speleothems, marine records).

## 698 **Acknowledgements**

699 We thank Stephan Mantel and Gerard Heuvelink at ISRIC World Soil Information  
700 (Wageningen, Netherlands), for sampling and provision of archived soil samples. We

701 thank Dr. Linfeng Gong, Mr. Shijin Zhao, Dr. Xinyue Dang and Dr. Jiantao Xue from  
702 China University of Geosciences (Wuhan) for their help during the field sampling in  
703 China. Huub Zwart, Vinothan Sivapalan, Caroline Bendle, George Bendle and Ryan  
704 Bendle are thanked for their participation in the USA field sampling campaign and  
705 Jessica Conway (University of Illinois Urbana Champaign), Chad Broyles and  
706 colleagues (International Ocean Discovery Programme - Texas A&M University) and  
707 Dr Amelia Shevenell (University of Southern Florida) and David Tubbs and Eimear  
708 Orgill (University of Birmingham) for help with equipment, logistics, shipping, sample  
709 handling and soil licenses. Thanks to Dr. Xing Xiang (Shangrao Normal University)  
710 for helping with the global map plotting. This work was supported by funding bodies  
711 in China and the UK, namely the National Natural Science Foundation of China (Grant  
712 Nos. 41830319, 41807419, 41821001, U20A2094, 91951208, 41773135), the Key  
713 R&D Project of Ministry of Science and Technology (grant no. 2016YFA0601100),  
714 the 111 project (National Bureau of Foreign Experts and the Ministry of Education of  
715 China; Grant No. BP20004), the Fundamental Research Funds for the National  
716 Universities, China University of Geosciences, Wuhan (Grant No. CUGL170815), the  
717 Leverhulme Trust (RPG-2018-110), the Birmingham-Illinois Partnership Fund, the  
718 UoB School of GEES Pump Priming Fund. We thank the China Scholarship Council  
719 (CSC) (Grant No. 201306410031) for supporting Canfa Wang's studies at the  
720 University of Birmingham and the UK's Natural Environmental Research Council  
721 (NERC) and the NERC CENTA-DTP (Central England NERC Training Alliance –  
722 Doctorial Training Partnership) for funding Alice Hardman's PhD studies and research  
723 training grant (NE/L002493/1) and for an independent research fellowship to Sarah  
724 Greene (NE/L011050/1). Ilya Mandel is a recipient of the Australian Research Council  
725 Future Fellowship FT190100574.

726

727 **Table and figure captions**

728 Fig. 1. Molecular structure of *normal*, *iso* and *anteiso* C<sub>15</sub> 3-OH-FAs.

729

730 Fig. 2. Maps showing the locations of soil samples used in this study. The colour  
731 spectrum of the dots illustrates the mean annual air temperature (MAAT) of each  
732 sampling site. A) Global overview map showing the locations of soil samples, with  
733 examples of C<sub>15</sub> 3-OH-FAs distributions in three soils, with markedly different MAATs,  
734 from Greenland (Sample GL005-2), China (Sample TJ-3), and Ghana (Sample GH002-  
735 02). The peaks in green in the inset chromatograph represent *normal* 3-OH-FA, the  
736 peaks in blue represent *anteiso* 3-OH-FA, the peaks in orange represent *iso* 3-OH-FA.  
737 B) Map showing the locations of soil samples from the eastern USA. C) Map showing  
738 the locations of soil samples from Southern Africa. D) Map showing the locations of  
739 soil samples from eastern China.

740

741 Fig. 3. Examples of distribution of 3-OH-FAs in soils from different mean annual air  
742 temperature (MAAT) and pH. The peaks in green represent *normal* 3-OH-FAs, the  
743 peaks in blue represent *anteiso* 3-OH-FAs, the peaks in red represent *iso* 3-OH-FAs.

744

745 Fig. 4. Heat map showing the Pearson correlation coefficients of 3-OH-FA based  
746 proxies and environmental parameters.

747



748 Fig. 5. Scatter-plots showing the relationship of 3-OH-FA based indices and mean  
749 annual air temperature (MAAT) and residuals. A) Global RAN<sub>15</sub> vs MAAT; B) Global  
750 RAN<sub>17</sub> vs MAAT. 95% observational and functional bounds are also shown. These  
751 represent a 95% probability that: a) a new observation and; b) the true function without  
752 observational errors will lie within the respective bounds.

753

754 Fig. 6. Scatter-plot showing the regional data points and regional linear calibrations for  
755 3-OH-FA based proxies vs MAAT (with the global linear regression line for  
756 comparison). Regression lines are not shown for regions where correlation is not  
757 significant ( $p > 0.05$ ). A) RAN<sub>15</sub> vs MAAT; B) RAN<sub>17</sub> vs MAAT.

758

759 Fig. 7. Scatter-plot showing the global relationship between 3-OH-FA based RIAN  
760 proxy vs soil pH and residuals. 95% observational and functional bounds are also  
761 shown. These represent a 95% probability that: a) a new observation and; b) the true  
762 function without observational errors will lie within the respective bounds.

763

764 Fig. 8 Scatter-plots showing the regional and global calibrations between RIAN and  
765 soil pH. Regression lines are not shown for regions where correlation is not significant  
766 ( $p > 0.05$ ).

767

768 Fig. 9. Comparison of 3-OH-FA based temperature proxies with GDGT based  
769 temperature proxies. A) RAN<sub>15</sub> and MBT'<sub>5ME</sub>-MAAT; B) RAN<sub>17</sub> and MBT'<sub>5ME</sub>-MAAT.

770 95% observational and functional bounds are also shown. These represent a 95%  
771 probability that: a) a new observation and; b) the true function without observational  
772 errors will lie within the respective bounds.

773

774 Fig. 10. Comparison of 3-OH-FA based pH proxies with GDGT based pH proxies. A)  
775 The linear correlation between Branching Ratio and CBT. B) The linear correlation  
776 between RIAN and CBT. C) The linear correlation between Branched Index and CBT.  
777 D) The linear correlation between RIN and CBT.

778

779 Fig. 11. A) Schematic of a Gaussian Process emulator (showing just 1 dimension of  
780 many); B) GP regression temperature predictions based on 3-OH-FA distributions vs  
781 true temperature in our new global soil data-set (see Fig. 12). The GP reduces the root  
782 mean square uncertainty on predictions compared to empirical regressions.

783

784 Fig. 12. Gaussian Process (GP) regression approach using all the 3-OH-FAs isomers  
785 ( $C_{10}$ - $C_{18}$ ) and just the  $C_{15}$  and  $C_{17}$  *iso*, *anteiso* and *normal* isomers for both temperature  
786 and pH. A) The GP regression temperature predictor as a function of the true  
787 temperature using all the isomers from  $C_{10}$  to  $C_{18}$ . B) The GP regression pH predictor  
788 as a function of the true pH using all the isomers from  $C_{10}$  to  $C_{18}$ . C) The GP regression  
789 temperature predictor as a function of the true temperature using just the  $C_{15}$  and  $C_{17}$   
790 *iso*, *anteiso* and *normal* isomers. D) The GP regression pH predictor as a function of  
791 the true pH using just the  $C_{15}$  and  $C_{17}$  *iso*, *anteiso* and *normal* isomers.

792

793 **References**

- 794 Bååth, E. and Anderson, T.H. (2003) Comparison of soil fungal/bacterial ratios in a  
795 pH gradient using physiological and PLFA-based techniques. *Soil Biology and*  
796 *Biochemistry* 35, 955-963.
- 797 Bahram, M., Hildebrand, F., Forslund, S.K., Anderson, J.L., Soudzilovskaia, N.A.,  
798 Bodegom, P.M., Bengtsson-Palme, J., Anslan, S., Coelho, L.P., Harend, H., Huerta-  
799 Cepas, J., Medema, M.H., Maltz, M.R., Mundra, S., Olsson, P.A., Pent, M., Polme,  
800 S., Sunagawa, S., Ryberg, M., Tedersoo, L. and Bork, P. (2018) Structure and  
801 function of the global topsoil microbiome. *Nature* 560, 233-237.
- 802 Bauersachs, T., Rochelmeier, J. and Schwark, L. (2015) Seasonal lake surface water  
803 temperature trends reflected by heterocyst glycolipid-based molecular thermometers.  
804 *Biogeosciences* 12, 3741-3751.
- 805 Bernardet, J.-F., Segers, P., Vancanneyt, M., Berthe, F., Kersters, K. and Vandamme,  
806 P. (1996) Cutting a Gordian knot: emended classification and description of the genus  
807 *Flavobacterium*, emended description of the family *Flavobacteriaceae*, and proposal  
808 of *Flavobacterium hydatis* nom. nov. (basonym, *Cytophaga aquatilis* Strohl and Tait  
809 1978). *International Journal of Systematic and Evolutionary Microbiology* 46, 128-  
810 148.
- 811 Blaga, C.I., Reichart, G.-J., Schouten, S., Lotter, A.F., Werne, J.P., Kosten, S.,  
812 Mazzeo, N., Lacerot, G. and Sinninghe Damsté, J.S. (2010) Branched glycerol dialkyl  
813 glycerol tetraethers in lake sediments: Can they be used as temperature and pH  
814 proxies? *Organic Geochemistry* 41, 1225-1234.

815 Blyth, A.J., Farrimond, P. and Jones, M. (2006) An optimised method for the  
816 extraction and analysis of lipid biomarkers from stalagmites. *Organic Geochemistry*  
817 37, 882-890.

818 Brassell, S., Eglinton, G., Marlowe, I., Pflaumann, U. and Sarnthein, M. (1986)  
819 Molecular stratigraphy: A new tool for climatic assessment. *Nature* 320, 129-133.

820 Cho, H., Tripathi, B.M., Moroenyane, I., Takahashi, K., Kerfahi, D., Dong, K. and  
821 Adams, J.M. (2019) Soil pH rather than elevation determines bacterial phylogenetic  
822 community assembly on Mt. Norikura. *FEMS Microbiology Ecology* 95, fiy216.

823 Chudinova, S.M., Frauenfeld, O.W., Barry, R.G., Zhang, T. and Sorokovikov, V.A.  
824 (2006) Relationship between air and soil temperature trends and periodicities in the  
825 permafrost regions of Russia. *Journal of Geophysical Research: Earth Surface* 111.

826 Davtian, N., Ménot, G., Bard, E., Poulencard, J. and Podwojewski, P. (2016)  
827 Consideration of soil types for the calibration of molecular proxies for soil pH and  
828 temperature using global soil datasets and Vietnamese soil profiles. *Organic*  
829 *Geochemistry* 101, 140-153.

830 de Bar, M.W., Weiss, G., Rampen, S., Lattaud, J., Bale, N.J., Brummer, G.-J.A.,  
831 Schulz, H., Rush, D., Kim, J.-H. and Donner, B. (2020) Global temperature  
832 calibration of the Long chain Diol Index in marine surface sediments. *Organic*  
833 *Geochemistry*, 103983.

834 De Jonge, C., Hopmans, E.C., Stadnitskaia, A., Rijpstra, W.I.C., Hofland, R.,  
835 Tegelaar, E. and Sinninghe Damsté, J.S. (2013) Identification of novel penta- and  
836 hexamethylated branched glycerol dialkyl glycerol tetraethers in peat using HPLC–  
837 MS2, GC–MS and GC–SMB-MS. *Organic Geochemistry* 54, 78-82.

838 De Jonge, C., Hopmans, E.C., Zell, C.I., Kim, J.-H., Schouten, S. and Sinninghe  
839 Damsté, J.S. (2014) Occurrence and abundance of 6-methyl branched glycerol dialkyl  
840 glycerol tetraethers in soils: Implications for palaeoclimate reconstruction.  
841 *Geochimica et Cosmochimica Acta* 141, 97-112.

842 Delgado-Baquerizo, M., Oliverio, A.M., Brewer, T.E., Benavent-González, A.,  
843 Eldridge, D.J., Bardgett, R.D., Maestre, F.T., Singh, B.K. and Fierer, N. (2018) A  
844 global atlas of the dominant bacteria found in soil. *Science* 359, 320-325.

845 Denich, T.J., Beaudette, L.A., Lee, H. and Trevors, J.T. (2003) Effect of selected  
846 environmental and physico-chemical factors on bacterial cytoplasmic membranes.  
847 *Journal of Microbiological Methods* 52, 149-182.

848 Dirghangi, S.S., Pagani, M., Hren, M.T. and Tipple, B.J. (2013) Distribution of  
849 glycerol dialkyl glycerol tetraethers in soils from two environmental transects in the  
850 USA. *Organic Geochemistry* 59, 49-60.

851 Dunkley Jones, T., Eley, Y.L., Thomson, W., Greene, S.E., Mandel, I., Edgar, K. and  
852 Bendle, J.A. (2020) OPTiMAL: a new machine learning approach for GDGT-based  
853 palaeothermometry. *Clim. Past* 16, 2599-2617.

854 Eglinton, G., Hunneman, D.H. and McCormick, A. (1968) Gas chromatographic—  
855 mass spectrometric studies of long chain hydroxy acids.—III. The mass spectra of the  
856 methyl esters trimethylsilyl ethers of aliphatic hydroxy acids. A facile method of  
857 double bond location. *Organic Mass Spectrometry* 1, 593-611.

858 Eglinton, T. and Eglinton, G. (2008) Molecular proxies for paleoclimatology. *Earth  
859 and Planetary Science Letters* 275, 1-16.

860 Fanin, N., Kardol, P., Farrell, M., Nilsson, M.-C., Gundale, M.J. and Wardle, D.A.  
861 (2019) The ratio of Gram-positive to Gram-negative bacterial PLFA markers as an  
862 indicator of carbon availability in organic soils. *Soil Biology and Biochemistry* 128,  
863 111-114.

864 Giotis, E.S., McDowell, D.A., Blair, I.S. and Wilkinson, B.J. (2007) Role of  
865 branched-chain fatty acids in pH stress tolerance in *Listeria monocytogenes*. *Applied*  
866 *and Environmental Microbiology* 73, 997-1001.

867 Goossens, H., Irene, W., Rijpstra, C., Düren, R., De Leeuw, J. and Schenck, P. (1986)  
868 Bacterial contribution to sedimentary organic matter; a comparative study of lipid  
869 moieties in bacteria and Recent sediments. *Organic Geochemistry* 10, 683-696.

870 Griffiths, R.I., Thomson, B.C., James, P., Bell, T., Bailey, M. and Whiteley, A.S.  
871 (2011) The bacterial biogeography of British soils. *Environmental microbiology* 13,  
872 1642-1654.

873 Haug, G.H., Ganopolski, A., Sigman, D.M., Rosell-Mele, A., Swann, G.E.,  
874 Tiedemann, R., Jaccard, S.L., Bollmann, J., Maslin, M.A. and Leng, M.J. (2005)  
875 North Pacific seasonality and the glaciation of North America 2.7 million years ago.  
876 *Nature* 433, 821-825.

877 Hedrick, D.B., Peacock, A.D., Lovley, D.R., Woodard, T.L., Nevin, K.P., Long, P.E.  
878 and White, D.C. (2009) Polar lipid fatty acids, LPS-hydroxy fatty acids, and  
879 respiratory quinones of three *Geobacter* strains, and variation with electron acceptor.  
880 *Journal of Industrial Microbiology & Biotechnology* 36, 205-209.

881 Hopmans, E.C., Schouten, S. and Sinninghe Damsté, J.S. (2016) The effect of  
882 improved chromatography on GDGT-based palaeoproxies. *Organic Geochemistry* 93,  
883 1-6.

884 Huang, X., Cui, J., Pu, Y., Huang, J. and Blyth, A.J. (2008) Identifying "free" and  
885 "bound" lipid fractions in stalagmite samples: An example from Heshang Cave,  
886 Southern China. *Applied Geochemistry* 23, 2589-2595.

887 Huang, X., Meyers, P.A., Jia, C., Zheng, M., Xue, J., Wang, X. and Xie, S. (2013)  
888 Paleotemperature variability in central China during the last 13 ka recorded by a novel  
889 microbial lipid proxy in the Dajihu peat deposit. *The Holocene* 23, 1123-1129.

890 Huguet, A., Coffinet, S., Roussel, A., Gayraud, F., Anquetil, C., Bergonzini, L.,  
891 Bonanomi, G., Williamson, D., Majule, A. and Derenne, S. (2019) Evaluation of 3-  
892 hydroxy fatty acids as a pH and temperature proxy in soils from temperate and  
893 tropical altitudinal gradients. *Organic Geochemistry* 129, 1-13.

894 Humphreys, G.O., Hancock, I.C. and Meadow, P.M. (1972) Synthesis of the  
895 hydroxyacids in lipid A of *Pseudomonas aeruginosa*. *Microbiology* 71, 221-230.

896 Ikemoto, S., Kuraishi, H., Komagata, K., Azuma, R., Suto, T. and Murooka, H.  
897 (1978) Cellular fatty acid composition in *Pseudomonas* species. *The Journal of*  
898 *General and Applied Microbiology* 24, 199-213.

899 IPCC (2014) *Climate Change 2014: Synthesis Report. Contribution of Working*  
900 *Groups I, II and III to the Fifth Assessment Report of the Intergovernmental Panel on*  
901 *Climate Change*. IPCC, Geneva, Switzerland.

902 Jenske, R. and Vetter, W. (2008) Gas chromatography/electron-capture negative ion  
903 mass spectrometry for the quantitative determination of 2-and 3-hydroxy fatty acids in  
904 bovine milk fat. *Journal of Agricultural and Food Chemistry* 56, 5500-5505.

905 Jones, R.T., Robeson, M.S., Lauber, C.L., Hamady, M., Knight, R. and Fierer, N.  
906 (2009) A comprehensive survey of soil acidobacterial diversity using pyrosequencing  
907 and clone library analyses. *The ISME Journal* 3, 442-453.

908 Kaneda, T. (1991) Iso- and anteiso-fatty acids in bacteria: biosynthesis, function, and  
909 taxonomic significance. *Microbiology and Molecular Biology Reviews* 55, 288-302.

910 Kawamura, K. and Ishiwatari, R. (1984) Tightly bound aliphatic acids in Lake Biwa  
911 sediments: Their origin and stability. *Organic Geochemistry* 7, 121-126.

912 Kim, J.-H., Schouten, S., Hopmans, E.C., Donner, B. and Sinninghe Damsté, J.S.  
913 (2008) Global sediment core-top calibration of the TEX<sub>86</sub> paleothermometer in the  
914 ocean. *Geochimica et Cosmochimica Acta* 72, 1154-1173.

915 Klages, J.P., Salzmann, U., Bickert, T., Hillenbrand, C.D., Gohl, K., Kuhn, G.,  
916 Bohaty, S.M., Titschack, J., Muller, J., Frederichs, T., Bauersachs, T., Ehrmann, W.,  
917 van de Flierdt, T., Pereira, P.S., Larter, R.D., Lohmann, G., Niezgodzki, I.,  
918 Uenzelmann-Neben, G., Zundel, M., Spiegel, C., Mark, C., Chew, D., Francis, J.E.,  
919 Nehrke, G., Schwarz, F., Smith, J.A., Freudenthal, T., Esper, O., Palike, H., Ronge,  
920 T.A., Dziadek, R. and Science Team of Expedition, P.S. (2020) Temperate rainforests  
921 near the South Pole during peak Cretaceous warmth. *Nature* 580, 81-86.

922 Klok, J., Baas, M., Cox, H.C., de Leeuw, J.W., Rijpstra, W.I.C. and Schenck, P.A.  
923 (1988) The mode of occurrence of lipids in a Namibian Shelf diatomaceous ooze with  
924 emphasis on the  $\beta$ -hydroxy fatty acids. *Organic Geochemistry* 12, 75-80.



925 Koga, Y. (2012) Thermal adaptation of the archaeal and bacterial lipid membranes.  
926 Archaea 2012, 789652.

927 Kumar, G.S., Jagannadham, M.V. and Ray, M.K. (2002) Low-temperature-induced  
928 changes in composition and fluidity of lipopolysaccharides in the antarctic  
929 psychrotrophic bacterium *Pseudomonas syringae*. Journal of Bacteriology 184, 6746-  
930 6749.

931 Lauber, C.L., Hamady, M., Knight, R. and Fierer, N. (2009) Pyrosequencing-based  
932 assessment of soil pH as a predictor of soil bacterial community structure at the  
933 continental scale. Applied and Environmental Microbiology 75, 5111-5120.

934 Lee, A.K.Y., Chan, C.K., Fang, M. and Lau, A.P.S. (2004) The 3-hydroxy fatty acids  
935 as biomarkers for quantification and characterization of endotoxins and Gram-  
936 negative bacteria in atmospheric aerosols in Hong Kong. Atmospheric Environment  
937 38, 6307-6317.

938 Lee, H.-G., An, D.-S., Im, W.-T., Liu, Q.-M., Na, J.-R., Cho, D.H., Jin, C.W., Lee, S.-  
939 T. and Yang, D.-C. (2007) *Chitinophaga ginsengisegetis* sp. nov. and *Chitinophaga*  
940 *ginsengisoli* sp. nov., isolated from soil of a ginseng field in South Korea.  
941 International Journal of Systematic and Evolutionary Microbiology 57, 1396-1401.

942 Lei, Y., Yang, H., Dang, X., Zhao, S. and Xie, S. (2016) Absence of a significant bias  
943 towards summer temperature in branched tetraether-based paleothermometer at two  
944 soil sites with contrasting temperature seasonality. Organic Geochemistry 94, 83-94.

945 Liu, W., Allison, S.D., Xia, J., Liu, L. and Wan, S. (2016) Precipitation regime drives  
946 warming responses of microbial biomass and activity in temperate steppe soils.  
947 Biology and Fertility of Soils 52, 469-477.

948 Luo, G., Yang, H., Algeo, T.J., Hallmann, C. and Xie, S. (2019) Lipid biomarkers for  
949 the reconstruction of deep-time environmental conditions. *Earth-Science Reviews*  
950 189, 99-124.

951 McElhaney, R.N., De Gier, J. and Van der Neut-Kok, E. (1973) The effect of  
952 alterations in fatty acid composition and cholesterol content on the nonelectrolyte  
953 permeability of *Acholeplasma laidlawii* B cells and derived liposomes. *Biochimica et*  
954 *Biophysica Acta (BBA)-Biomembranes* 298, 500-512.

955 Meyers, P.A. (1997) Organic geochemical proxies of paleoceanographic,  
956 paleolimnologic, and paleoclimatic processes. *Organic Geochemistry* 27, 213-250.

957 Mielniczuk, Z., Mielniczuk, E. and Larsson, L. (1993) Gas chromatography-mass  
958 spectrometry methods for analysis of 2- and 3-hydroxylated fatty acids: Application  
959 for endotoxin measurement. *Journal of Microbiological Methods* 17, 91-102.

960 Mitchell, P. (1966) Chemiosmotic coupling in oxidative and photosynthetic  
961 phosphorylation. *Biological Reviews* 41, 445-501.

962 Miyagawa, E., Azuma, R. and Suto, T. (1979) Cellular fatty acid composition in  
963 Gram-negative obligately anaerobic rods. *The Journal of General and Applied*  
964 *Microbiology* 25, 41-51.

965 Naafs, B.D.A., Gallego-Sala, A.V., Inglis, G.N. and Pancost, R.D. (2017) Refining  
966 the global branched glycerol dialkyl glycerol tetraether (brGDGT) soil temperature  
967 calibration. *Organic Geochemistry* 106, 48-56.

968 Naafs, B.D.A., Hefter, J. and Stein, R. (2012) Application of the long chain diol index  
969 (LDI) paleothermometer to the early Pleistocene (MIS 96). *Organic Geochemistry* 49,  
970 83-85.

971 Nagle, J. and Morowitz, H. (1978) Molecular mechanisms for proton transport in  
972 membranes. *Proceedings of the National Academy of Sciences* 75, 298-302.

973 Oliverio, A.M., Bradford, M.A. and Fierer, N. (2017) Identifying the microbial taxa  
974 that consistently respond to soil warming across time and space. *Global Change*  
975 *Biology* 23, 2117-2129.

976 Oyaizu, H. and Komagata, K. (1983) Grouping of *Pseudomonas* species on the basis  
977 of cellular fatty acid composition and the quinone system with special reference to the  
978 existence of 3-hydroxy fatty acids. *The Journal of General and Applied Microbiology*  
979 29, 17-40.

980 Peterse, F., van der Meer, J., Schouten, S., Weijers, J.W.H., Fierer, N., Jackson, R.B.,  
981 Kim, J.-H. and Sinninghe Damsté, J.S. (2012) Revised calibration of the MBT–CBT  
982 paleotemperature proxy based on branched tetraether membrane lipids in surface  
983 soils. *Geochimica et Cosmochimica Acta* 96, 215-229.

984 Prahl, F.G. and Wakeham, S.G. (1987) Calibration of unsaturation patterns in long-  
985 chain ketone compositions for palaeotemperature assessment. *Nature* 330, 367-369.

986 Raetz, C.R., Reynolds, C.M., Trent, M.S. and Bishop, R.E. (2007) Lipid A  
987 modification systems in gram-negative bacteria. *Annu. Rev. Biochem.* 76, 295-329.

988 Rampen, S.W., Willmott, V., Kim, J.-H., Uliana, E., Mollenhauer, G., Schefuß, E.,  
989 Sinninghe Damsté, J.S. and Schouten, S. (2012) Long chain 1,13- and 1,15-diols as a

990 potential proxy for palaeotemperature reconstruction. *Geochimica et Cosmochimica*  
991 *Acta* 84, 204-216.

992 Rasmussen, C.E. and Nickisch, H. (2010) Gaussian processes for machine learning  
993 (GPML) toolbox. *Journal of Machine Learning Research* 11, 3011-3015.

994 Rasmussen, C.E. and Williams, C.K.I. (2006) Gaussian processes for machine  
995 learning. The MIT Press, Massachusetts.

996 Rousk, J., Bååth, E., Brookes, P.C., Lauber, C.L., Lozupone, C., Caporaso, J.G.,  
997 Knight, R. and Fierer, N. (2010) Soil bacterial and fungal communities across a pH  
998 gradient in an arable soil. *The ISME Journal* 4, 1340-1351.

999 Russell, N. (1995) Psychrotrophy and adaptation to low temperatures: microbial  
1000 membrane lipids, *Proceedings of the 19th International Congress on Refrigeration:*  
1001 *Workshop Refrigeration and Microbiology: Health, Food, Drinks and Flowers*, pp.  
1002 359-365.

1003 Russell, N. and Fukunaga, N. (1990) A comparison of thermal adaptation of  
1004 membrane lipids in psychrophilic and thermophilic bacteria. *FEMS Microbiology*  
1005 *Letters* 75, 171-182.

1006 Sachs, J.P., Anderson, R.F. and Lehman, S.J. (2001) Glacial surface temperatures of  
1007 the southeast Atlantic Ocean. *Science* 293, 2077-2079.

1008 Schouten, S., Hopmans, E., Schefuß, E. and Sinninghe Damsté, J. (2002)  
1009 Distributional variations in marine crenarchaeotal membrane lipids: a new tool for  
1010 reconstructing ancient sea water temperatures? *Earth and Planetary Science Letters*  
1011 204, 265-274.

1012 Schouten, S., Hopmans, E.C. and Sinninghe Damsté, J.S. (2013) The organic  
1013 geochemistry of glycerol dialkyl glycerol tetraether lipids: A review. *Organic*  
1014 *Geochemistry* 54, 19-61.

1015 Siliakus, M.F., van der Oost, J. and Kengen, S.W.M. (2017) Adaptations of archaeal  
1016 and bacterial membranes to variations in temperature, pH and pressure. *Extremophiles*  
1017 21, 651-670.

1018 Singh, D., Shi, L. and Adams, J.M. (2013) Bacterial diversity in the mountains of  
1019 south-west China: climate dominates over soil parameters. *Journal of Microbiology*  
1020 51, 439-447.

1021 Suutari, M. and Laakso, S. (1994) Microbial fatty acids and thermal adaptation.  
1022 *Critical Reviews in Microbiology* 20, 285-328.

1023 Szponar, B., Krasnik, L., Hryniewiecki, T., Gamian, A. and Larsson, L. (2003)  
1024 Distribution of 3-hydroxy fatty acids in tissues after intraperitoneal injection of  
1025 endotoxin. *Clinical Chemistry* 49, 1149-1153.

1026 Szponar, B., Norin, E., Midtvedt, T. and Larsson, L. (2002) Limitations in the use of  
1027 3-hydroxy fatty acid analysis to determine endotoxin in mammalian samples. *Journal*  
1028 *of Microbiological Methods* 50, 283-289.

1029 Tyagi, P., Kawamura, K., Bikkina, S., Mochizuki, T. and Aoki, K. (2016) Hydroxy  
1030 fatty acids in snow pit samples from Mount Tateyama in central Japan: Implications  
1031 for atmospheric transport of microorganisms and plant waxes associated with Asian  
1032 dust. *Journal of Geophysical Research: Atmospheres* 121, 13641-13660.

1033 Tyagi, P., Yamamoto, S. and Kawamura, K. (2015) Hydroxy fatty acids in fresh snow  
1034 samples from northern Japan: long-range atmospheric transport of Gram-negative  
1035 bacteria by Asian winter monsoon. *Biogeosciences* 12, 7071-7080.

1036 Véquaud, P., Derenne, S., Thibault, A., Anquetil, C., Bonanomi, G., Collin, S.,  
1037 Contreras, S., Nottingham, A., Sabatier, P., Salinas, N., Scott, W.P., Werne, J.P. and  
1038 Huguet, A. (2020) Development of global temperature and pH calibrations based on  
1039 bacterial 3-hydroxy fatty acids in soils. *Biogeosciences Discussion* 2020, 1-40.

1040 Volkman, J.K., Barrett, S.M. and Blackburn, S.I. (1999) Fatty acids and hydroxy fatty  
1041 acids in three species of freshwater eustigmatophytes. *Journal of Phycology* 35, 1005-  
1042 1012.

1043 Volkman, J.K., Johns, R.B., Gillan, F.T., Perry, G.J. and Bavor Jr, H.J. (1980)  
1044 Microbial lipids of an intertidal sediment--I. Fatty acids and hydrocarbons.  
1045 *Geochimica et Cosmochimica Acta* 44, 1133-1143.

1046 Wakeham, S.G. (1999) Monocarboxylic, dicarboxylic and hydroxy acids released by  
1047 sequential treatments of suspended particles and sediments of the Black Sea. *Organic*  
1048 *Geochemistry* 30, 1059-1074.

1049 Wakeham, S.G., Pease, T.K. and Benner, R. (2003) Hydroxy fatty acids in marine  
1050 dissolved organic matter as indicators of bacterial membrane material. *Organic*  
1051 *Geochemistry* 34, 857-868.

1052 Wang, C., Bendle, J., Yang, Y., Yang, H., Sun, H., Huang, J. and Xie, S. (2016)  
1053 Impacts of pH and temperature on soil bacterial 3-hydroxy fatty acids: Development  
1054 of novel terrestrial proxies. *Organic Geochemistry* 94, 21-31.

1055 Wang, C., Bendle, J.A., Zhang, H., Yang, Y., Liu, D., Huang, J., Cui, J. and Xie, S.  
1056 (2018) Holocene temperature and hydrological changes reconstructed by bacterial 3-  
1057 hydroxy fatty acids in a stalagmite from central China. *Quaternary Science Reviews*  
1058 192, 97-105.

1059 Wang, C., Zhang, H., Huang, X., Huang, J. and Xie, S. (2012) Optimization of acid  
1060 digestion conditions on the extraction of fatty acids from stalagmites. *Frontiers of*  
1061 *Earth Science* 6, 109-114.

1062 Wang, H., An, Z., Lu, H., Zhao, Z. and Liu, W. (2020) Calibrating bacterial tetraether  
1063 distributions towards in situ soil temperature and application to a loess-paleosol  
1064 sequence. *Quaternary Science Reviews* 231.

1065 Weber, Y., De Jonge, C., Rijpstra, W.I.C., Hopmans, E.C., Stadnitskaia, A., Schubert,  
1066 C.J., Lehmann, M.F., Sinninghe Damsté, J.S. and Niemann, H. (2015) Identification  
1067 and carbon isotope composition of a novel branched GDGT isomer in lake sediments:  
1068 Evidence for lacustrine branched GDGT production. *Geochimica et Cosmochimica*  
1069 *Acta* 154, 118-129.

1070 Weijers, J.W.H., Schouten, S., van den Donker, J.C., Hopmans, E.C. and Sinninghe  
1071 Damsté, J.S. (2007) Environmental controls on bacterial tetraether membrane lipid  
1072 distribution in soils. *Geochimica et Cosmochimica Acta* 71, 703-713.

1073 Wikström, M., Sharma, V., Kaila, V.R.I., Hosler, J.P. and Hummer, G. (2015) New  
1074 perspectives on proton pumping in cellular respiration. *Chem Rev* 115, 2196-2221.

1075 Wilkinson, S.G., Galbraith, L. and Lightfoot, G.A. (1973) Cell walls, lipids, and  
1076 lipopolysaccharides of *Pseudomonas* species. *European Journal of Biochemistry* 33,  
1077 158-174.

1078 Wollenweber, H.-W. and Rietschel, E.T. (1990) Analysis of lipopolysaccharide (lipid  
1079 A) fatty acids. *Journal of Microbiological Methods* 11, 195-211.

1080 Wollenweber, H., Rietschel, E.T., Hofstad, T., Weintraub, A. and Lindberg, A. (1980)  
1081 Nature, type of linkage, quantity, and absolute configuration of (3-hydroxy) fatty  
1082 acids in lipopolysaccharides from *Bacteroides fragilis* NCTC 9343 and related strains.  
1083 *Journal of Bacteriology* 144, 898-903.

1084 Wollenweber, H.W., Seydel, U., Lindner, B., Lüderitz, O. and Rietschel, E.T. (1984)  
1085 Nature and location of amide-bound (R)-3-acyloxyacyl groups in lipid A of  
1086 lipopolysaccharides from various Gram-negative bacteria. *European Journal of*  
1087 *Biochemistry* 145, 265-272.

1088 Yang, H., Ding, W., Wang, J., Jin, C., He, G., Qin, Y. and Xie, S. (2012) Soil pH  
1089 impact on microbial tetraether lipids and terrestrial input index (BIT) in China.  
1090 *Science China Earth Sciences* 55, 236-245.

1091 Yang, H., Pancost, R.D., Dang, X., Zhou, X., Evershed, R.P., Xiao, G., Tang, C., Gao,  
1092 L., Guo, Z. and Xie, S. (2014) Correlations between microbial tetraether lipids and  
1093 environmental variables in Chinese soils: Optimizing the paleo-reconstructions in  
1094 semi-arid and arid regions. *Geochimica et Cosmochimica Acta* 126, 49-69.

1095 Yang, Y., Wang, C., Bendle, J.A., Yu, X., Gao, C., Lü, X., Ruan, X., Wang, R. and  
1096 Xie, S. (2020) A new sea surface temperature proxy based on bacterial 3-hydroxy  
1097 fatty acids. *Organic Geochemistry* 141, 103975.

1098 Yang, Y., Wang, C., Zhang, H., Huang, J. and Xie, S. (2016) Influence of extraction  
1099 methods on the distribution pattern and concentration of fatty acids and hydroxy fatty



1100 acids in soil samples: Acid digestion versus saponification. *Geochemical Journal* 50,  
1101 439-443.

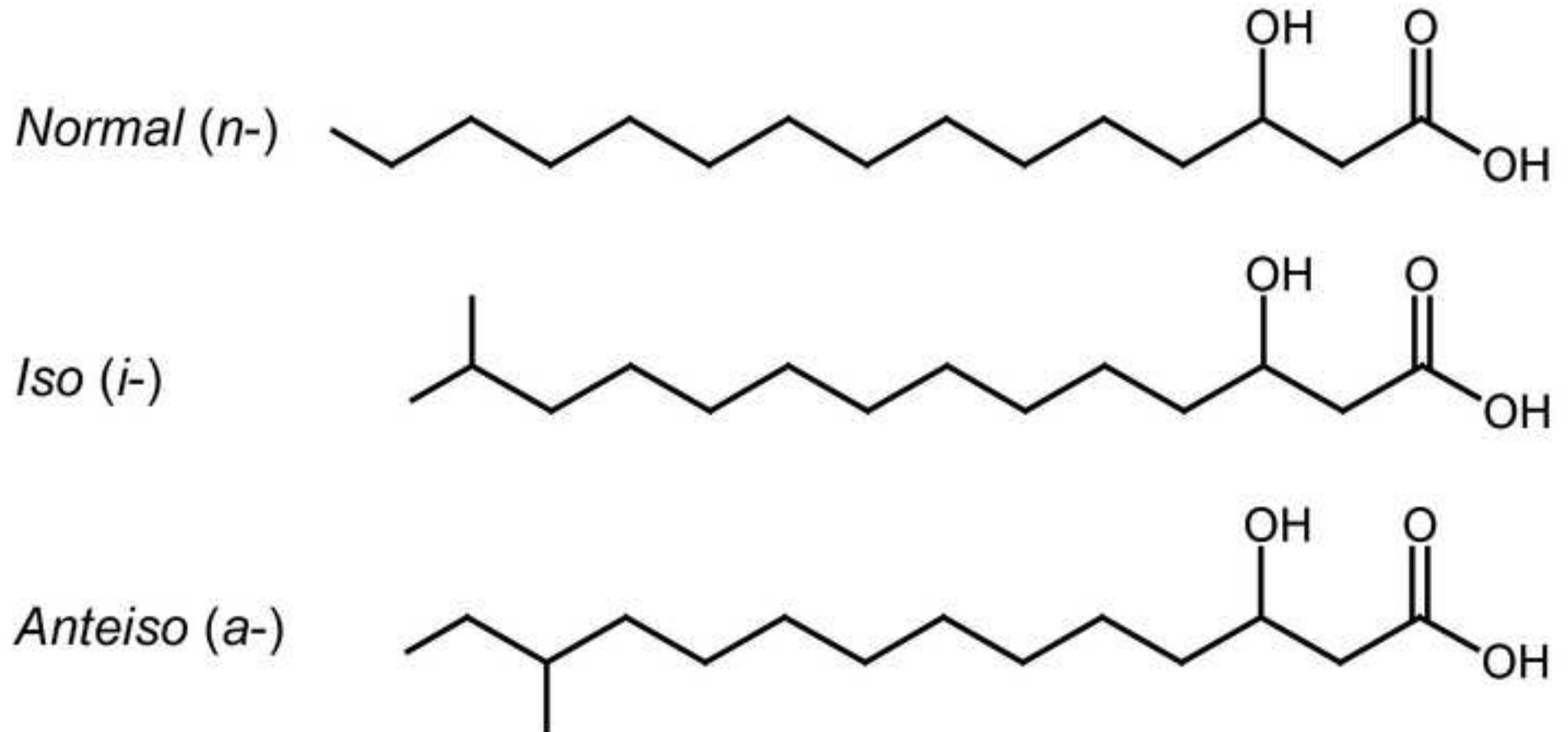
1102 Yao, M., Rui, J., Niu, H., Heděnc, P., Li, J., He, Z., Wang, J., Cao, W. and Li, X.  
1103 (2017) The differentiation of soil bacterial communities along a precipitation and  
1104 temperature gradient in the eastern Inner Mongolia steppe. *Catena* 152, 47-56.

1105 Zelles, L. (1999) Fatty acid patterns of phospholipids and lipopolysaccharides in the  
1106 characterisation of microbial communities in soil: a review. *Biology and Fertility of*  
1107 *Soils* 29, 111-129.

1108 Zhang, Y., Cong, J., Lu, H., Li, G., Xue, Y., Deng, Y., Li, H., Zhou, J. and Li, D.  
1109 (2015) Soil bacterial diversity patterns and drivers along an elevational gradient on  
1110 Shennongjia Mountain, China. *Microbial Biotechnology* 8, 739-746.

1111 Zhang, Z., Metzger, P. and Sachs, J.P. (2014) Bound lipid biomarkers in sediments  
1112 from El Junco Lake, Galápagos Islands. *Organic Geochemistry* 75, 122-128.

1113



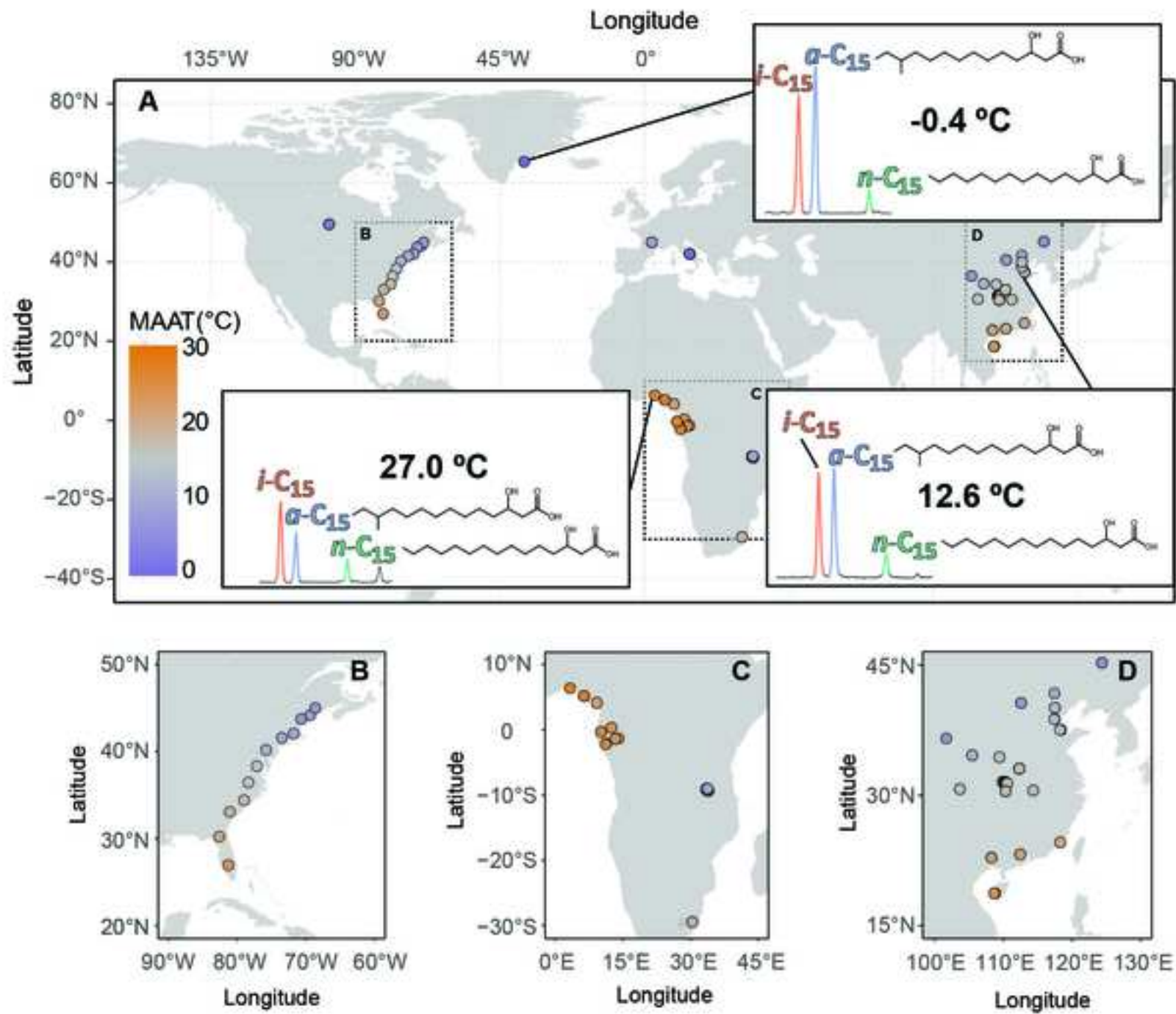


Figure 3

[Click here to access/download;Figure;Figure 3 Example of distributions V5.jpg](#)

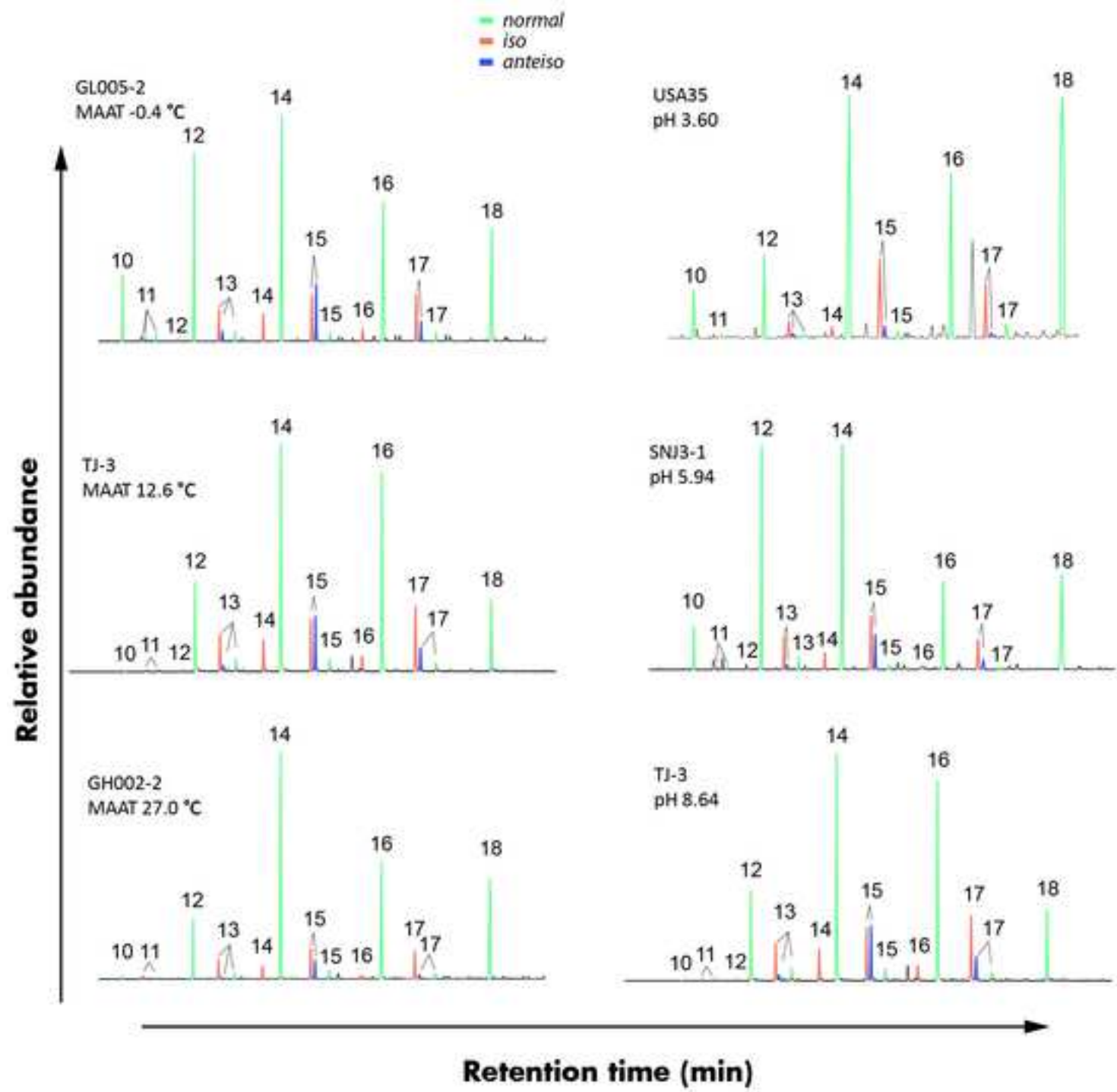
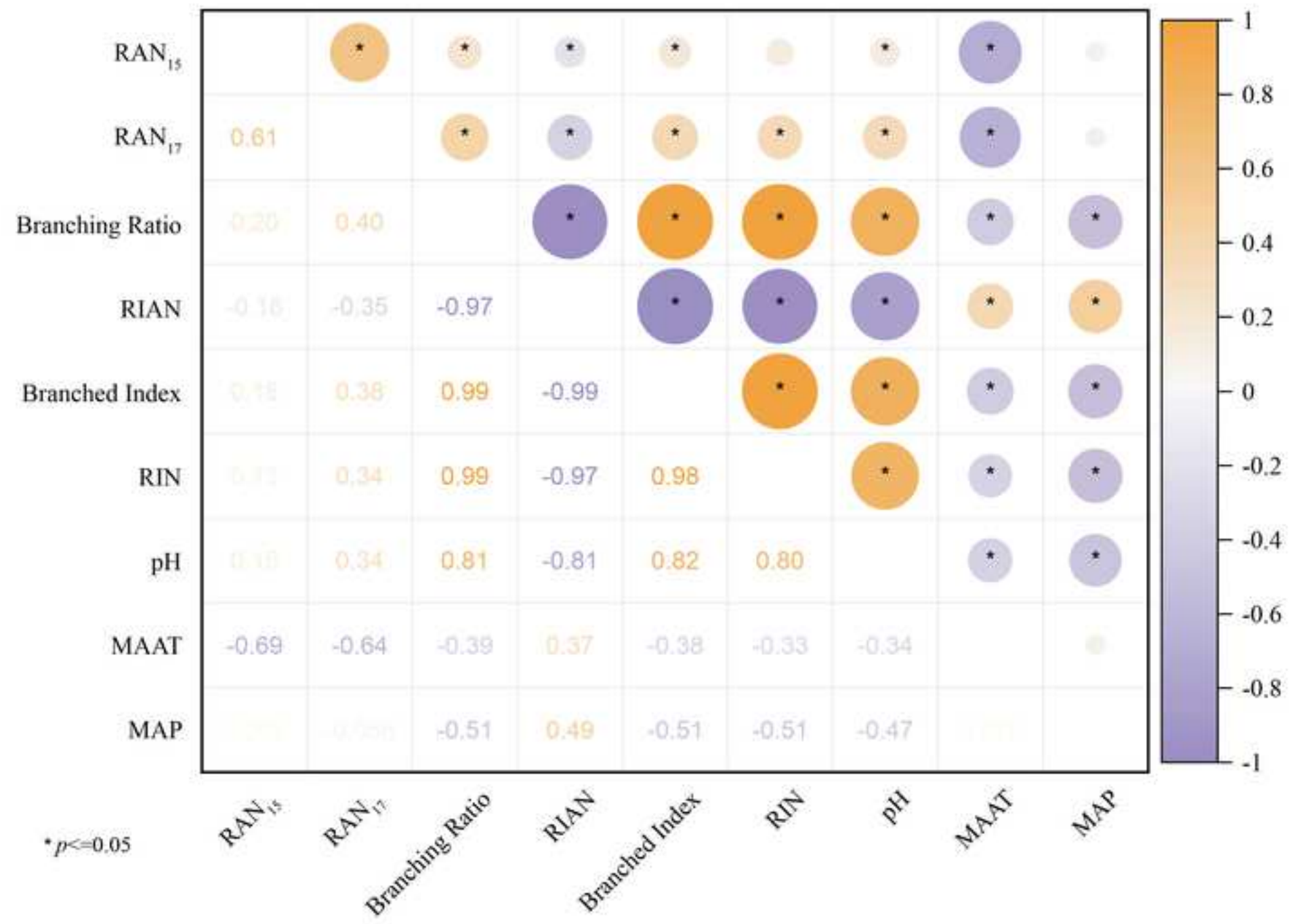


Figure 4

[Click here to access/download;Figure;Figure 4 Pearson coefficients.jpg](#)



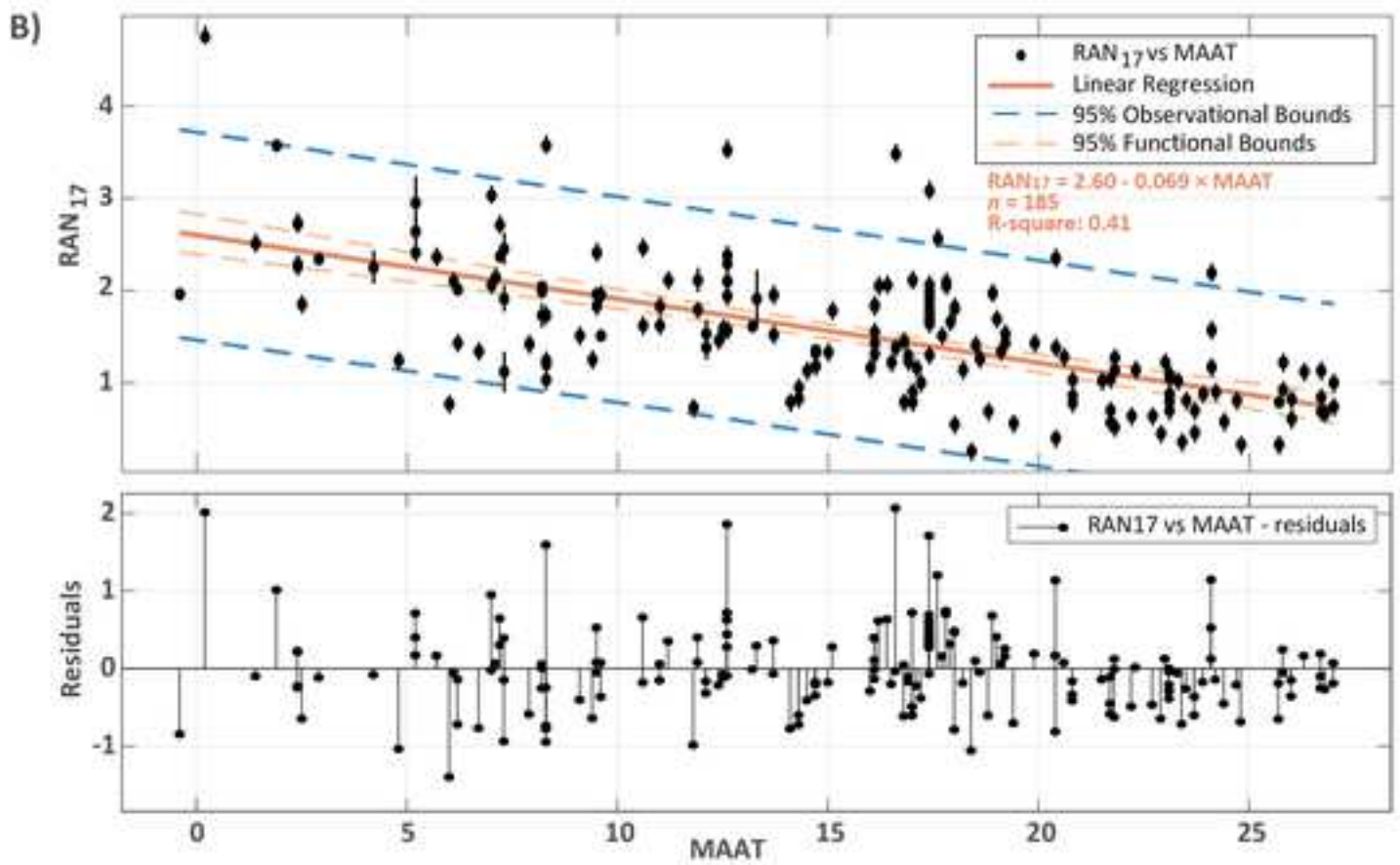
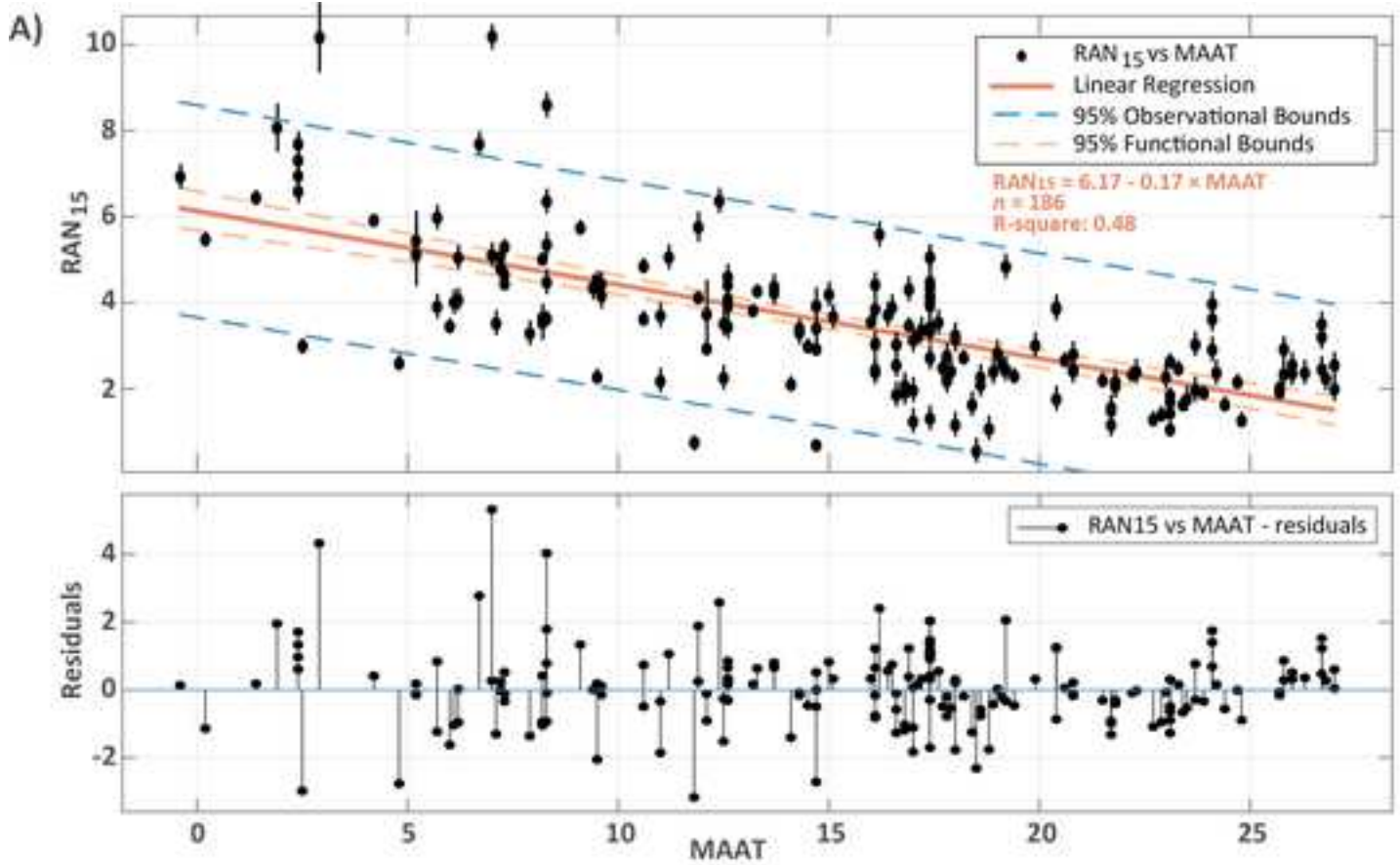




Figure 6

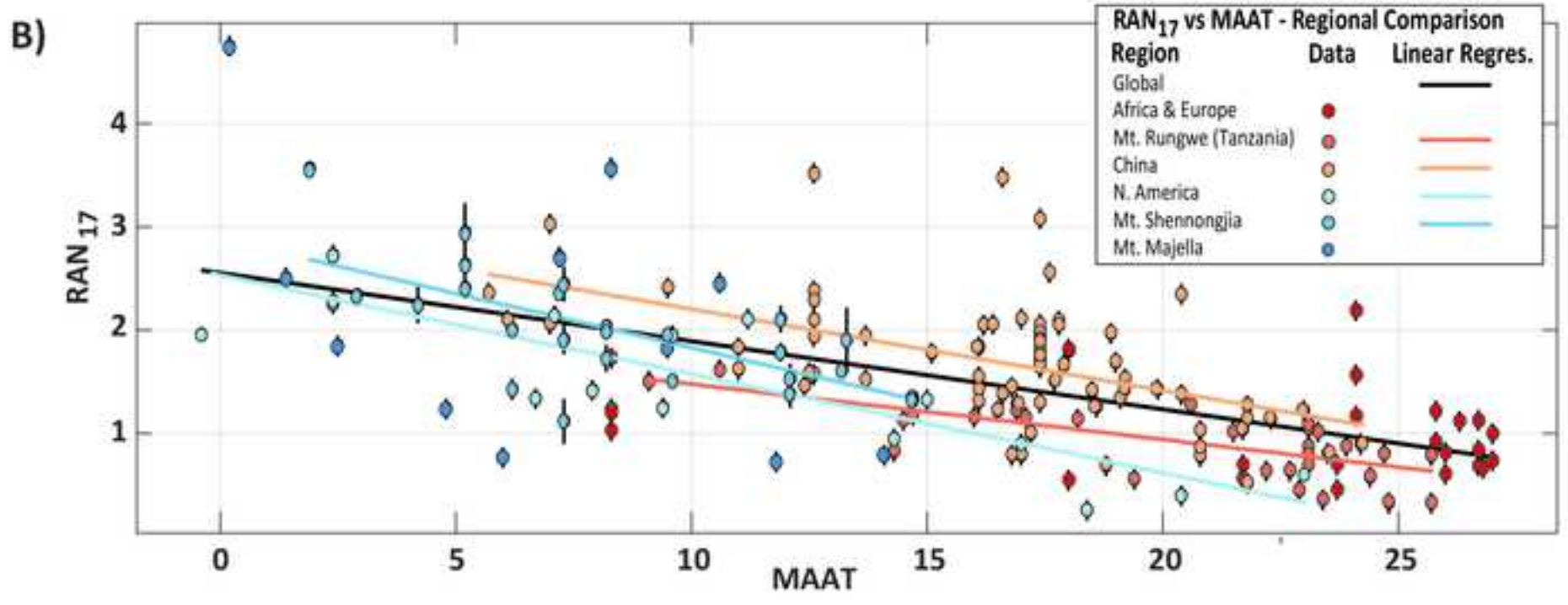
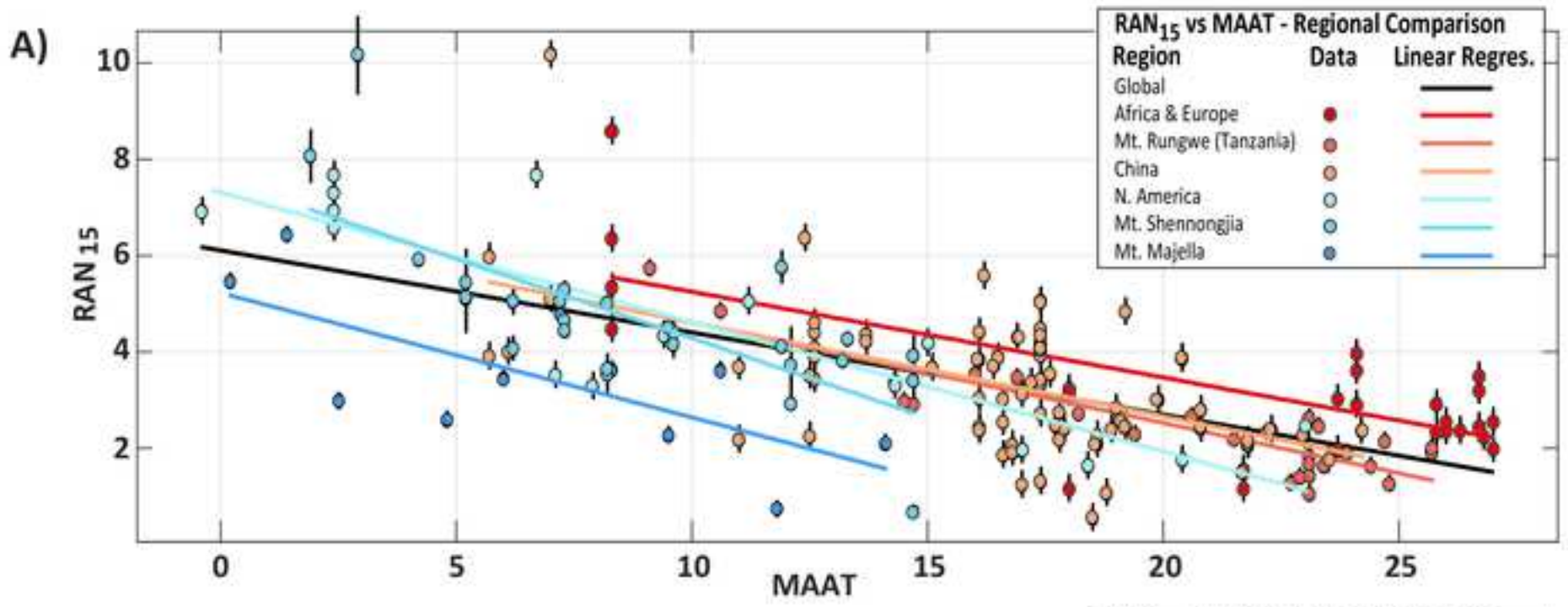


Figure 7

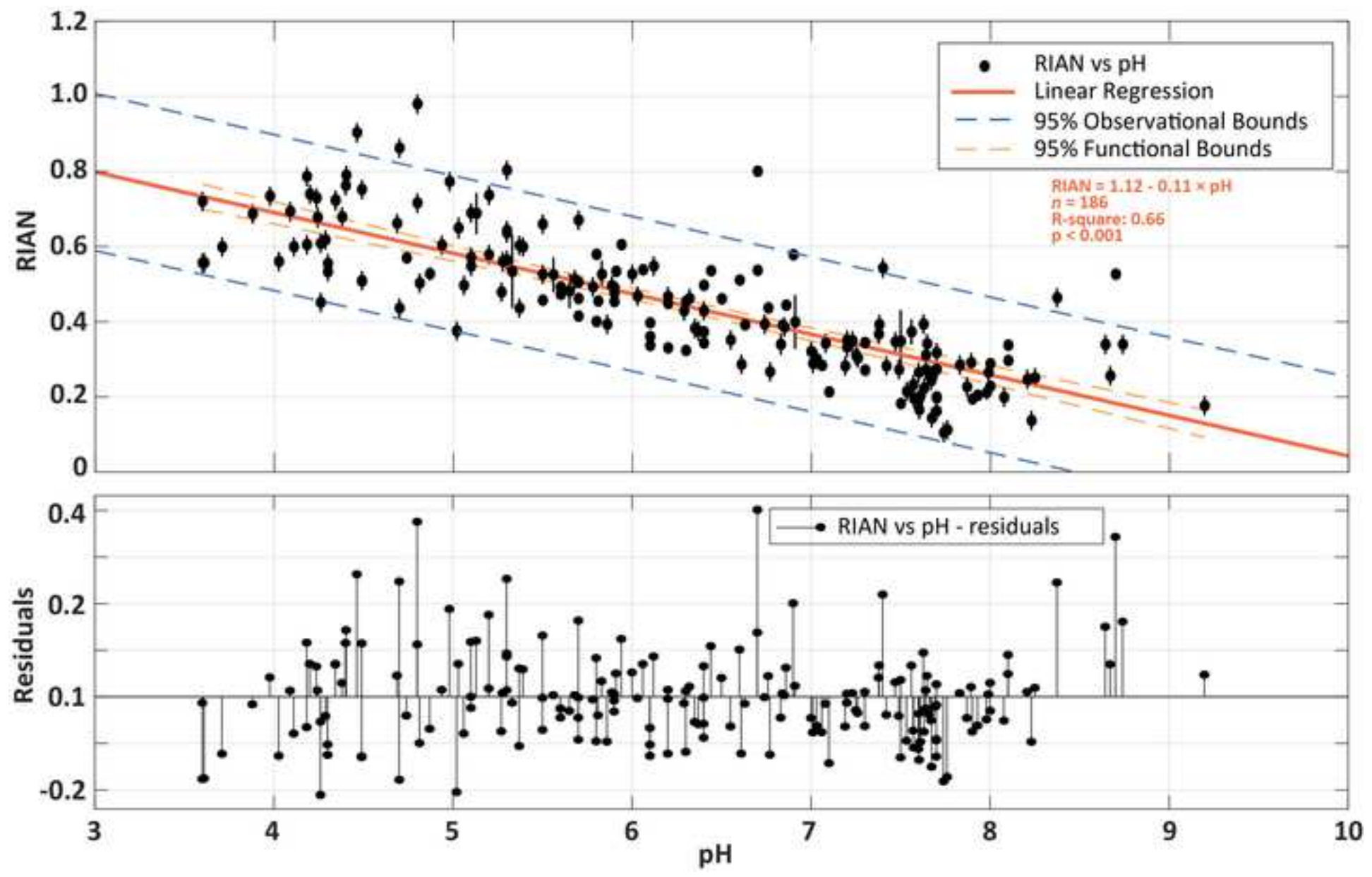
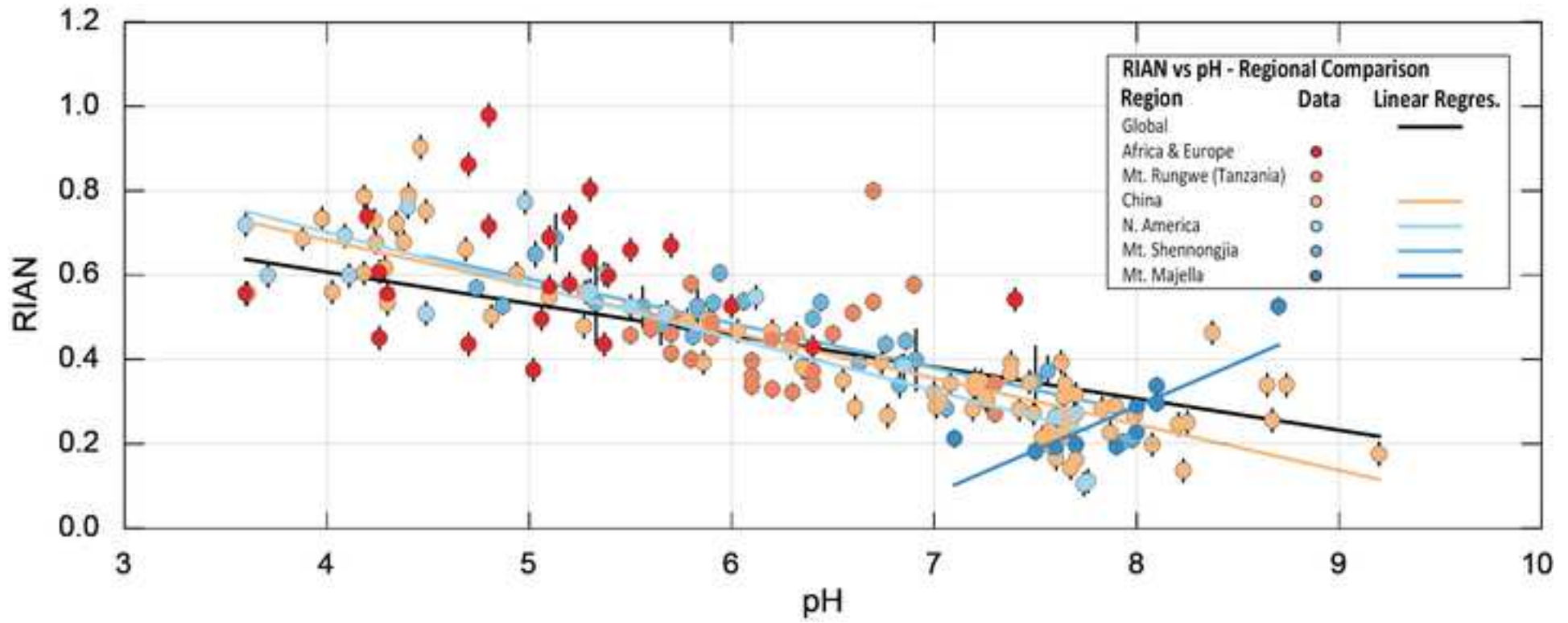
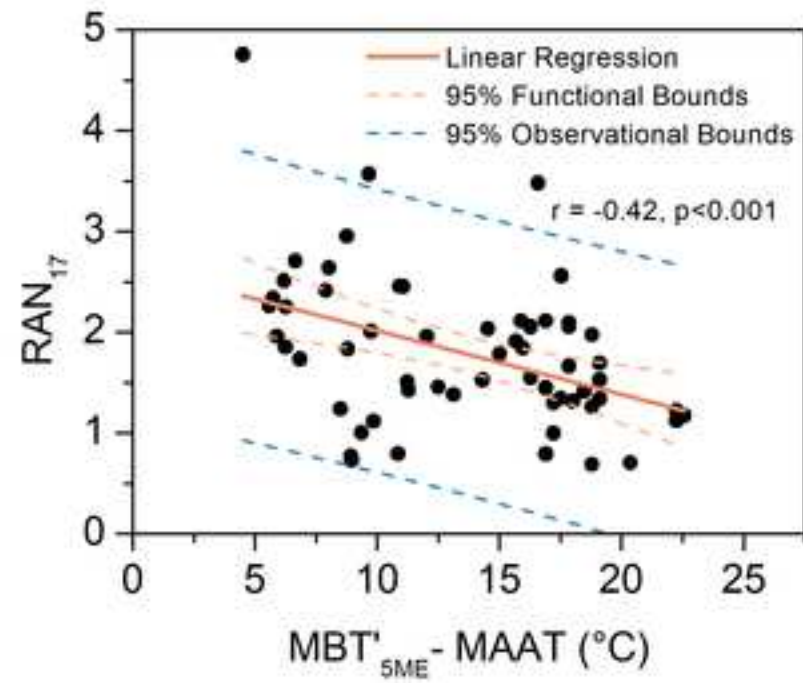
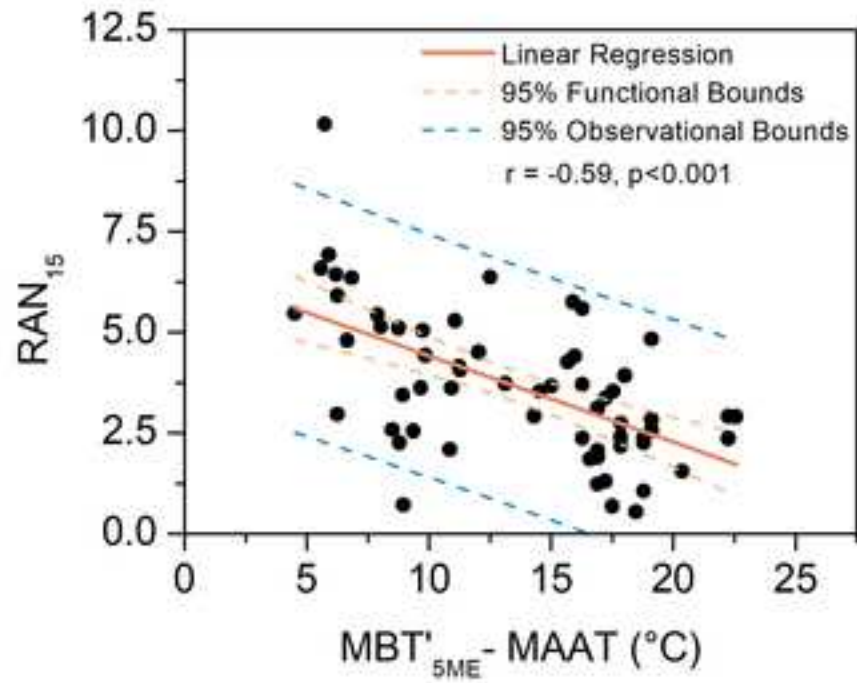
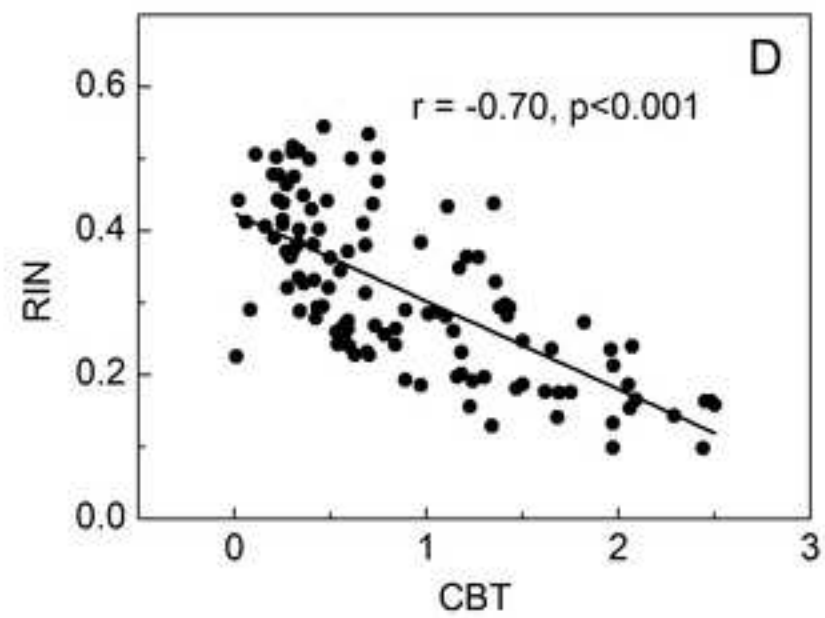
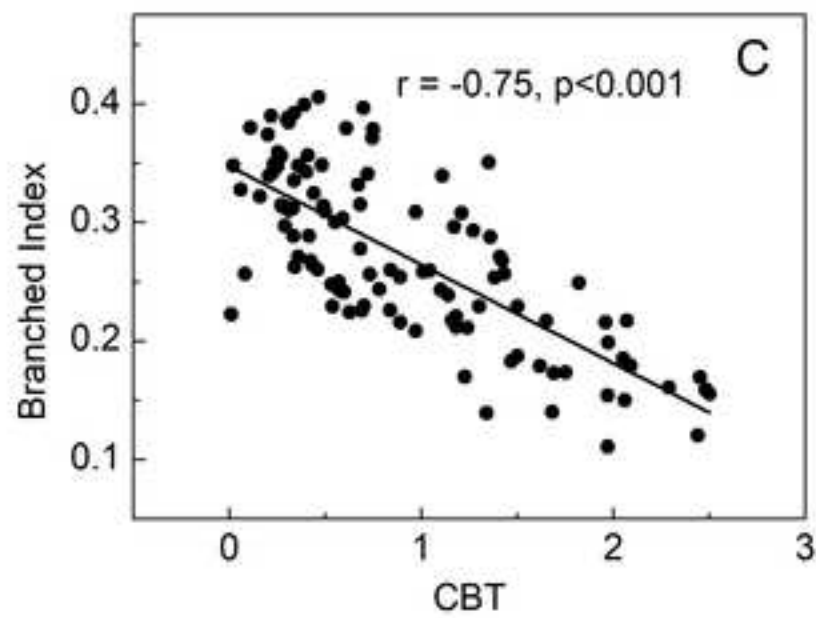
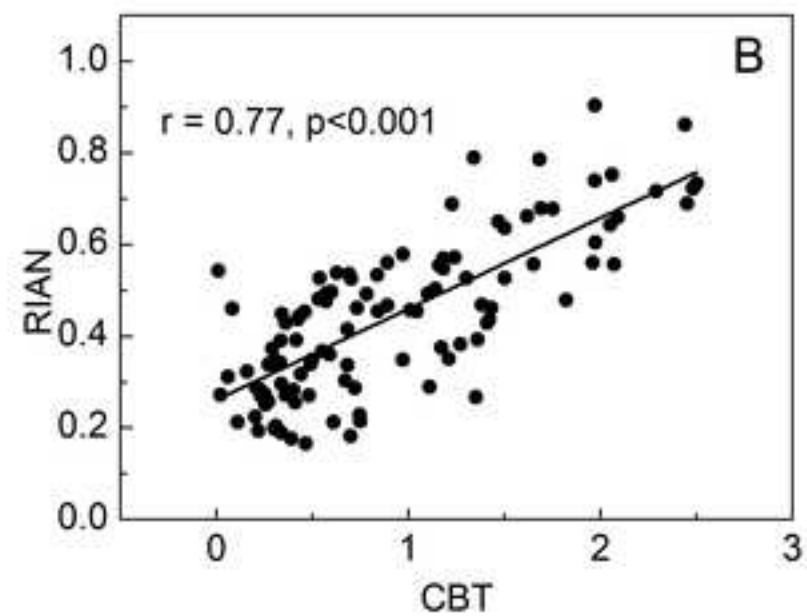
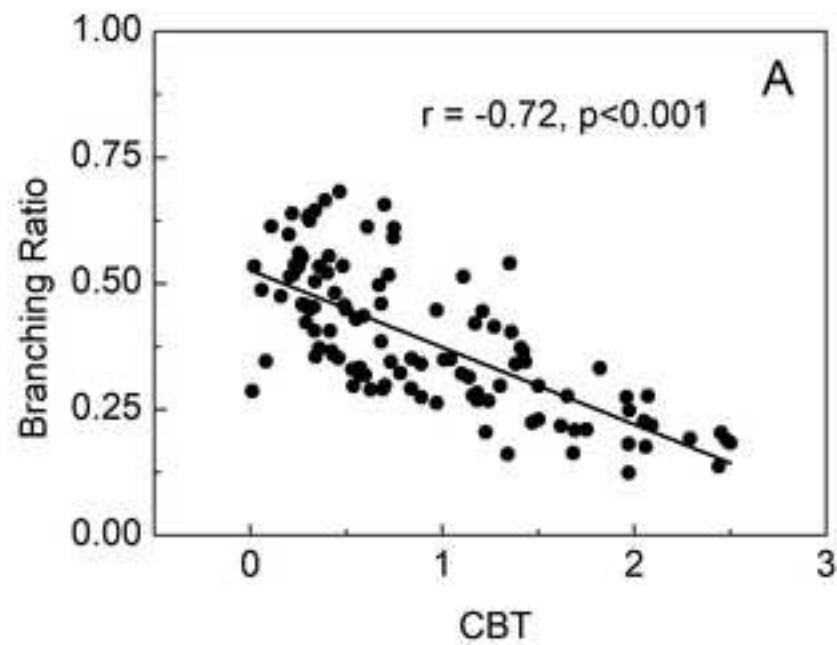


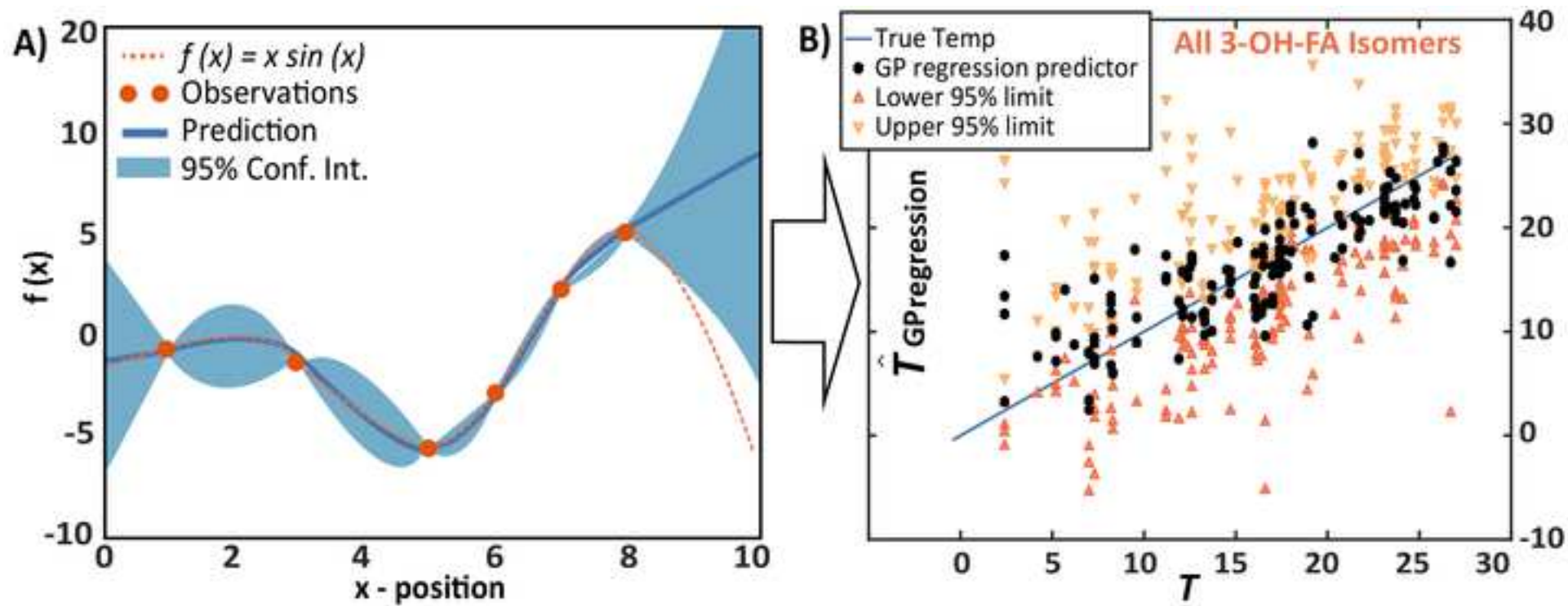


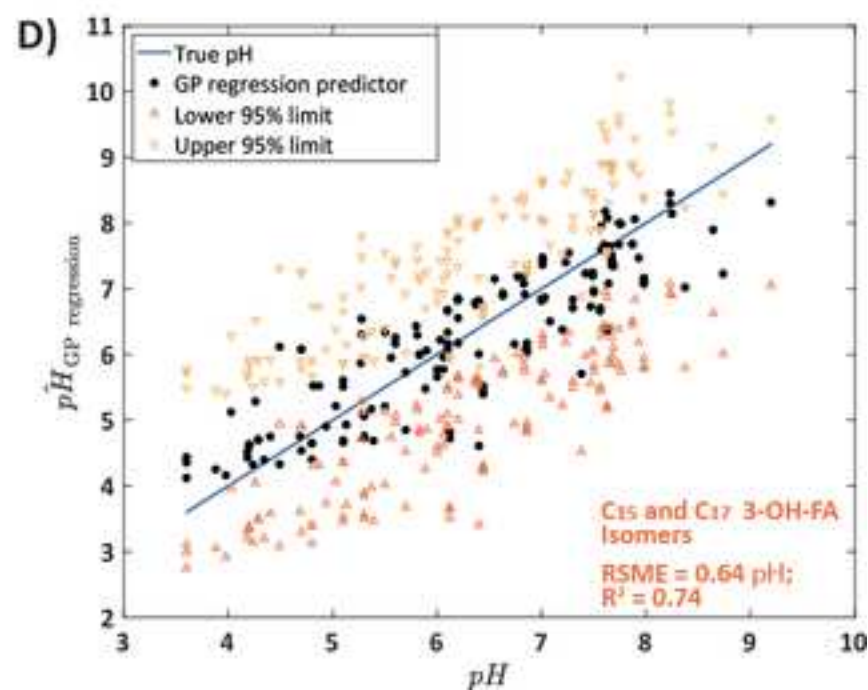
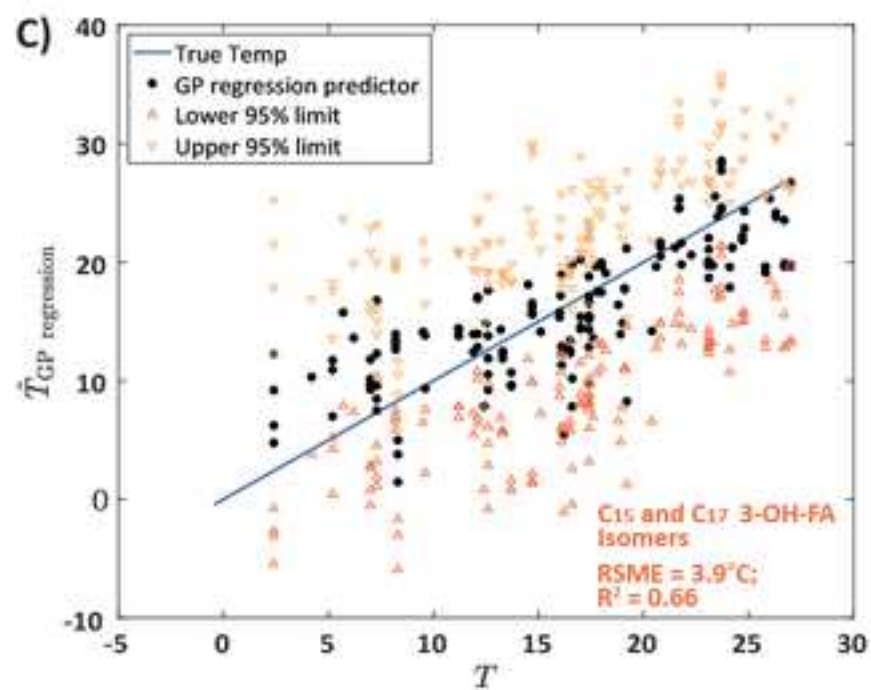
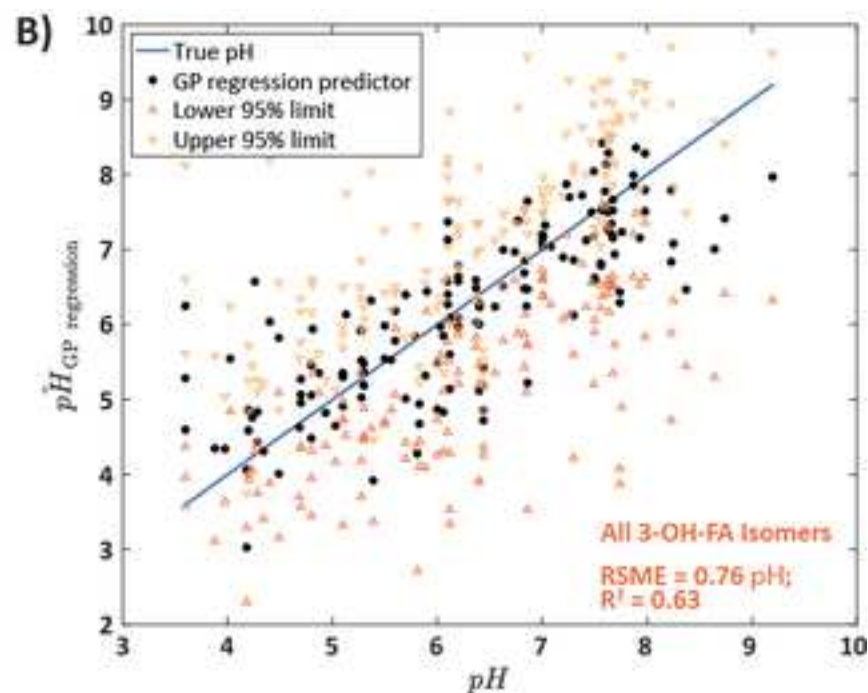
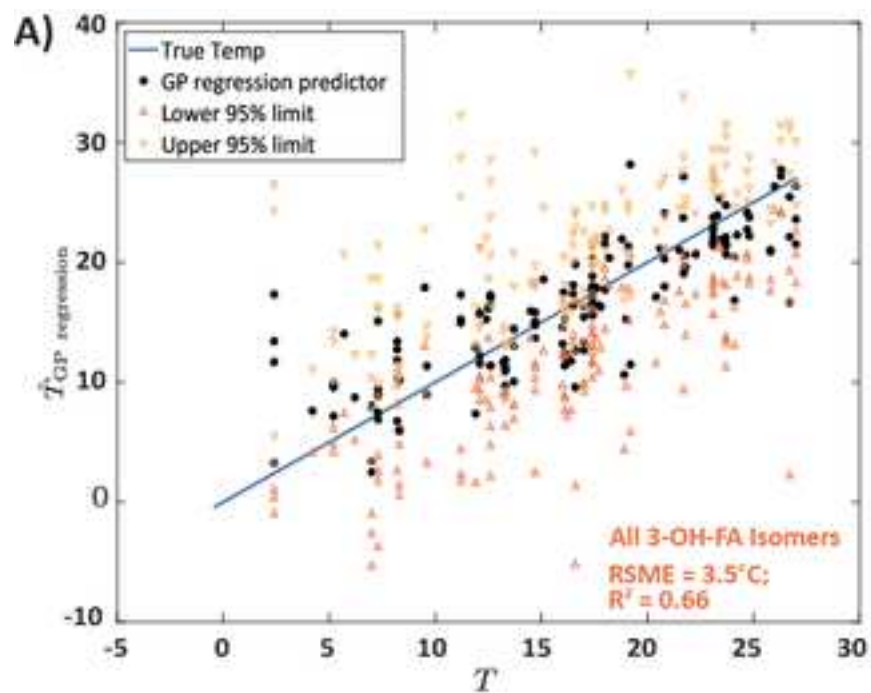
Figure 8













Click here to access/download  
**Appendix**  
Supplementary Data.xlsx

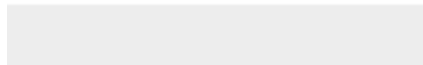




[Click here to access/download](#)

**Appendix**

[Supplementary Information-revision-clean.docx](#)





The authors declare no competing financial or non-financial interests.